

Supporting information

Highly Fluorescent Room Temperature Liquid Crystalline S-Annulated Swallow Tail Perylene Bisimide exhibiting Enhanced Electroluminescence (EQE > 11%)

Paresh Kumar Behera,^a Sushanta Lenka,^b Feng-Rong Chen,^b Prakalp Gautam,^b Iram Siddiqui,^b D. S. Shankar Rao,^c Jwo-Huei Jou*^b, and Ammathnadu Sudhakar Achalkumar*^{a,d}

^a*Department of Chemistry, Indian Institute of Technology Guwahati, Guwahati, 781039, Assam, India.*

^b*Department of Materials Science and Engineering National Tsing Hua University 101, Sec. 2, Kuang-Fu Road, Hsinchu 30013, Taiwan*

^c*Centre for Nano and Soft Matter Sciences, Arkavathi Campus, Survey No.7, Shivanapura, Dasanapura Hobli, Bengaluru – 562162, India.*

^d*Centre for Sustainable Polymers, Indian Institute of Technology Guwahati, Guwahati, 781039, Assam, India.*

Table of Contents

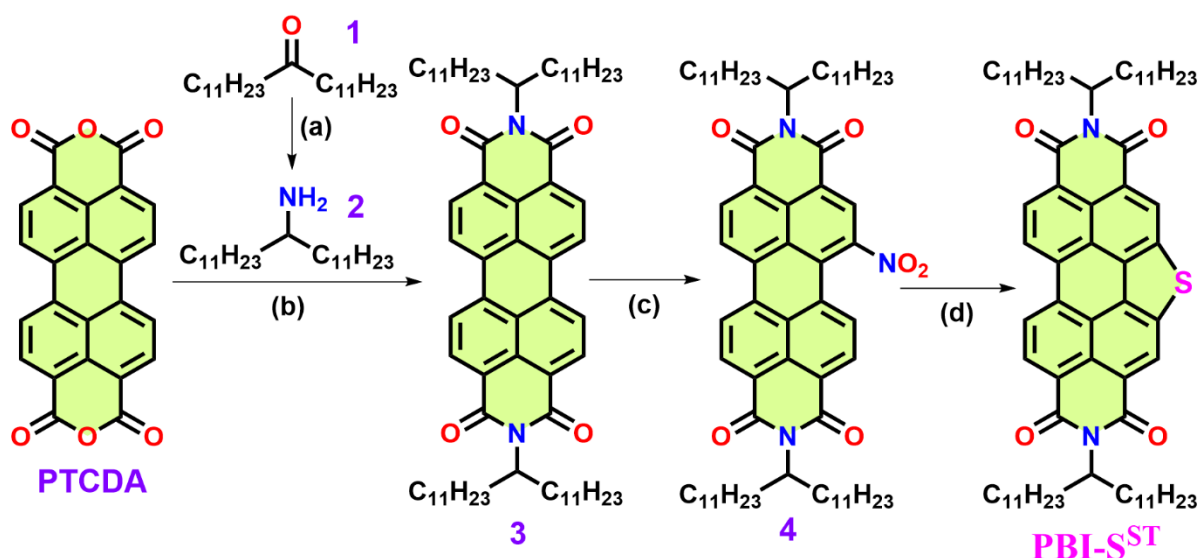
Serial Number	Contents	Page numbers
1	Materials and methods	S3
2	Experimental Section	S4-S6
3	NMR Spectra	S7-S8
4	MALDI-TOF Mass spectra	S9
5	Thermogravimetric analysis	S10
6	Differential Scanning Calorimetry	S10
7	Polarized Optical Microscopy	S11
8	X-ray diffraction studies	S11-S13
9	Photophysical studies	S14
10	Quantum yield measurement	S14-S15
11	Cyclic Voltammetry	S15
12	Device Fabrication and characterization	S16-S18
13	Surface Morphology Studies (AFM)	S18
14	DFT Studies	S18-S21
15	TD-DFT and NTO calculations	S21-S24
16	Electron-hole correlation plots for the individual states	S25-S26
17	Solvatochromism	S26-S27
18	Time resolved photoluminescence studies	S28
19	References	S29-S30

1. Materials and methods

Commercially available chemicals were utilized without further purification, and standard procedures were followed to dry the solvents. Chromatography was conducted using either silica gel (60-120 mesh) or neutral aluminum oxide. For thin-layer chromatography, aluminum sheets pre-coated with silica gel were employed. IR spectra were acquired at room temperature using a Perkin Elmer IR spectrometer (PerkinElmer UATR TWO). The spectral positions are reported in wave number (cm^{-1}) units. NMR spectra were recorded using a 600MHz Nuclear Magnetic Resonance (NMR) Spectrometer (Make: Bruker, Model: AVANCE III HD). Chemical shifts in ^1H NMR spectra were referenced to TMS as an internal standard and reported in ppm. Coupling constants were provided in Hz. Mass spectra were obtained using a MALDI-TOF mass spectrometer (Matrix Assisted Laser Desorption Ionization- Time of Flight, Make: BRUKER Model: AUTOFLEX SPEED) with α -Cyano-4-hydroxycinnamic acid as a matrix. The liquid crystalline behavior of the mesogenic compounds, including birefringence and fluidity, was investigated using a polarizing optical microscope (Nikon Eclipse LV100POL) equipped with a programmable hot stage (Mettler Toledo FP90). Observations were made with clean glass slides and coverslips. Differential scanning calorimetry (DSC) under a nitrogen atmosphere was used to determine transition temperatures and associated enthalpy changes. A Mettler Toledo DSC1 instrument was employed, and the peak temperatures corresponding to transitions obtained from DSC were consistent with the polarizing optical microscopic observations. The first heating and cooling cycles were conducted at a rate of $5\text{ }^\circ\text{C}/\text{min}$, and the transition temperatures were recorded. Variable temperature XRD studies were performed using samples filled in Lindemann capillaries. A high-resolution X-ray powder diffractometer (PANalytical X'Pert PRO) equipped with a high-resolution fast detector PIXCEL was used. The sample temperature was controlled using a Mettler hot stage/programmer (FP82HT/FP90). Thermogravimetric analysis (TGA) was carried out using a thermogravimetric analyzer (Mettler Toledo, model TG/SDTA 851 e) under a nitrogen flow at a heating rate of $10\text{ }^\circ\text{C}/\text{min}$. UV-Vis spectra were recorded using a Perkin-Elmer Lambda 750 UV/VIS/NIR spectrometer. Fluorescence emission in solution state was investigated using either a Horiba Fluoromax-4 fluorescence spectrophotometer or a Perkin Elmer LS 50B spectrometer. The absolute photoluminescence quantum efficiencies (PLQYs) of the neat or doped films were determined using an integrating sphere under an N_2 atmosphere. Cyclic Voltammetry (CV) studies were conducted using a Metrohm Autolab PGSTAT204 Electrochemical workstation with the assistance of NOVA software.

2. Experimental Section

2.1. Synthetic Scheme 1:



Reagents and conditions: (a) NH_4OAc , NaBH_3CN , MeOH, RT, 72 h (95%); (b) **2**, $\text{Zn}(\text{OAc})_2$, imidazole, 160 °C, 2h, (92%); (c) NaNO_2 , HNO_3 , 0 °C, 30 min., rt, 1 h (91%); (d) sulfur powder, anh. NMP, N_2 , 70 °C, 0.5 h, 180 °C, 12 h (74%).

2.2 Synthetic Procedure:

2.2.1 Synthetic route of Tricosan-12-amine (**2**):^{S1}

A 250 mL round-bottom flask was charged with 12-tricosanone (**1**) (5 g, 14.76 mmol), NH_4OAc (11.35 g, 147.6 mmol), NaBH_3CN (1.275 g, 1.38 mmol) and MeOH (100 mL) and stirred at room temperature (r.t.) for 72 h, until the starting material was consumed (monitored by TLC). The reaction was quenched by drop wise addition of conc. HCl (~12 mL) and the solvents removed by rotary evaporation. The resulting white solid was dissolved in H_2O (200 mL) and adjust to ~pH 10 with KOH, then extracted with CHCl_3 (3× 150 mL) to give desired product as a white solid (4.8g, 95.6%). $^1\text{H-NMR}$ (600MHz, CDCl_3): δ = 0.88 (t, 6H), 1.10-1.50 (m, 42H), 2.68 ppm (s, 1H).

2.2.2 Synthetic route of N, N-bis(Tricosan-12-amine)-perylene-3,4,9,10-tetracarboxylic Bisimide, (PBIST) (**3**):^{S1}

A mixture of perylene-3,4,9,10-tetracarboxylic dianhydride PTCDA (**3**) (2 g, 5.09 mmol), $\text{Zn}(\text{OAc})_2$ (0.35 g, 1.61 mmol), imidazole (5 g) and tricosan-12-amine (3.548 g, 10.44 mmol) was vigorously stirred at 160 °C for 5h. After cooling to r.t. the mixture was dissolved in minimum amount of THF and precipitated in 1000 mL of 1N HCl/MeOH 2:1 v/v. The orange red precipitate was collected by filtration, washed with H_2O followed by MeOH, dried at 80

°C in vacuum and further purified by silica flash-column chromatography with CHCl₃. The final product was recrystallized by chloroform-methanol system and obtained as orange solid (4.86 g, 92.1%). ¹H NMR (600 MHz, CDCl₃, ppm): δ 8.67 (s, 2H), 8.63 (s, 2H), 8.60-8.59 (s, 4H), 5.20-5.15 (m, 2H), 2.27-2.17 (m, 4H), 1.87-1.86 (m, 4H), 1.31-1.19 (m, 72H), 0.83 (t, *J* = 6 Hz, 12H). ¹³C NMR (150 MHz, CDCl₃, ppm): δ 164.4, 163.57, 134.49, 131.89, 131.12, 129.59, 126.43, 123.94, 123.20, 123.00, 54.77, 32.37, 31.91, 29.62, 29.61, 29.55, 29.33, 26.97, 22.67, 22.55, 14.10. MALDI-TOF exact mass calculated for C₇₀H₁₀₃N₂O₄ (M+H)⁺: 1035.78, found: 1035.367.

2.2.3 Synthetic route of N, N-bis(Tricosan-12-amine)-1-nitroperylene-3,4,9,10-tetracarboxydianhydride (4):^{S2}

In a round bottom flask, compound **3** (2 g, 1.93 mmol) was dissolved in CH₂Cl₂ (150 mL) and NaNO₂ (0.13 g, 1.93 mmol) was added to it. Then conc. HNO₃ (2.62 mL, 62.4 mmol) was added dropwise to the reaction mixture was stirred at 0 °C for 20-25 min. Then it was allowed to stir at rt. TLC was used for indicating completion of reaction. The reaction was quenched by adding H₂O (90 mL). The layers were separated and the aqueous phase was extracted with CH₂Cl₂ (3 times). The organic phases were combined, washed with water (3 times), dried over anhydrous Na₂SO₄ and concentrated under reduced pressure. The residue was purified through silica gel column chromatography (CHCl₃/Petroleum Ether 1:1) to afford compound **4** as a dark red solid (1.95 g, 90.8%). ¹H NMR (600 MHz, CDCl₃, ppm): δ 8.80-8.71 (m, 5H), 8.61-8.58 (m, 1H), 8.26 (d, *J* = 6 Hz, 1H), 5.16 (m, 2H), 2.22 (t, *J* = 6 Hz, 4H), 1.85 (t, *J* = 6 Hz, 4H), 1.25-1.20 (m, 72H), 0.84 (t, *J* = 6 Hz, 12H).

2.2.5 Synthetic route of N, N-bis(Tricosan-12-amine)-S-annulated perylene-3,4,9,10-tetracarboxydianhydride (PBI-SST):

A mixture of compound (**4**) (1 g, 0.92 mmol) and Sulfur powder (.30 g, 9.2 mmol) was heated to dissolve in *N*-methylpyrrolidone (20 mL) at 70 °C for 30 min. and then refluxed at 180 °C under Ar atmosphere for overnight until the starting material could not be detected by TLC. After cooling to room temperature, 2M HCl was added, then the precipitate was filtered, washed with water and dried. The crude product was purified by column chromatography on neutral alumina. Elution with 5-10 % CHCl₃-Hexanes system followed by 20% CHCl₃-Hexane system yields the desired product in good yield. Further purification was done by addition of concentrate solution of compound in cold methanol gives the waxy product (0.730 g, 74%).

$R_f = 0.6$ (10% CHCl_3 -Hexane); IR: ν_{max} in cm^{-1} : 2952, 2920, 2851, 1694, 1651, 1596, 1559, 1454, 1426, 1361, 1347, 1302, 1243, 1234, 1199, 1162, 1115, 911, 840, 808, 742, 721; ^1H NMR (600 MHz, CDCl_3 , ppm): δ 9.24-9.19 (m, 2H), 8.85-8.80 (m, 4H), 5.30 (m, 2H), 2.36-2.30 (m, 4H), 1.94-1.93 (m, 4H), 1.24-1.17 (m, 72H), 0.82-0.80 (t, $J = 6$ Hz, 12H). ^{13}C NMR (150 MHz, CDCl_3 , ppm): δ 165.15, 164.72, 163.97, 163.65, 138.08, 133.00, 132.24, 130.03, 129.28, 127.87, 127.09, 126.13, 123.37, 122.96, 122.66, 122.25, 55.07, 32.49, 31.89, 29.72, 27.63, 29.32, 27.10, 22.65, 14.09. MALDI-TOF exact mass calculated for $\text{C}_{70}\text{H}_{101}\text{N}_2\text{O}_4\text{S}$ ($\text{M}+\text{H}^+$): 1065.7482, found: 1065.7496. Elemental analysis ($\text{C}_{70}\text{H}_{100}\text{N}_2\text{O}_4\text{S}$): C: 78.90%, H: 9.46%, N: 2.63%, S: 3.01% (Expected); C: 79.26%, H: 9.51%, N: 2.82%, S: 2.87% (Observed).

3. NMR Spectra

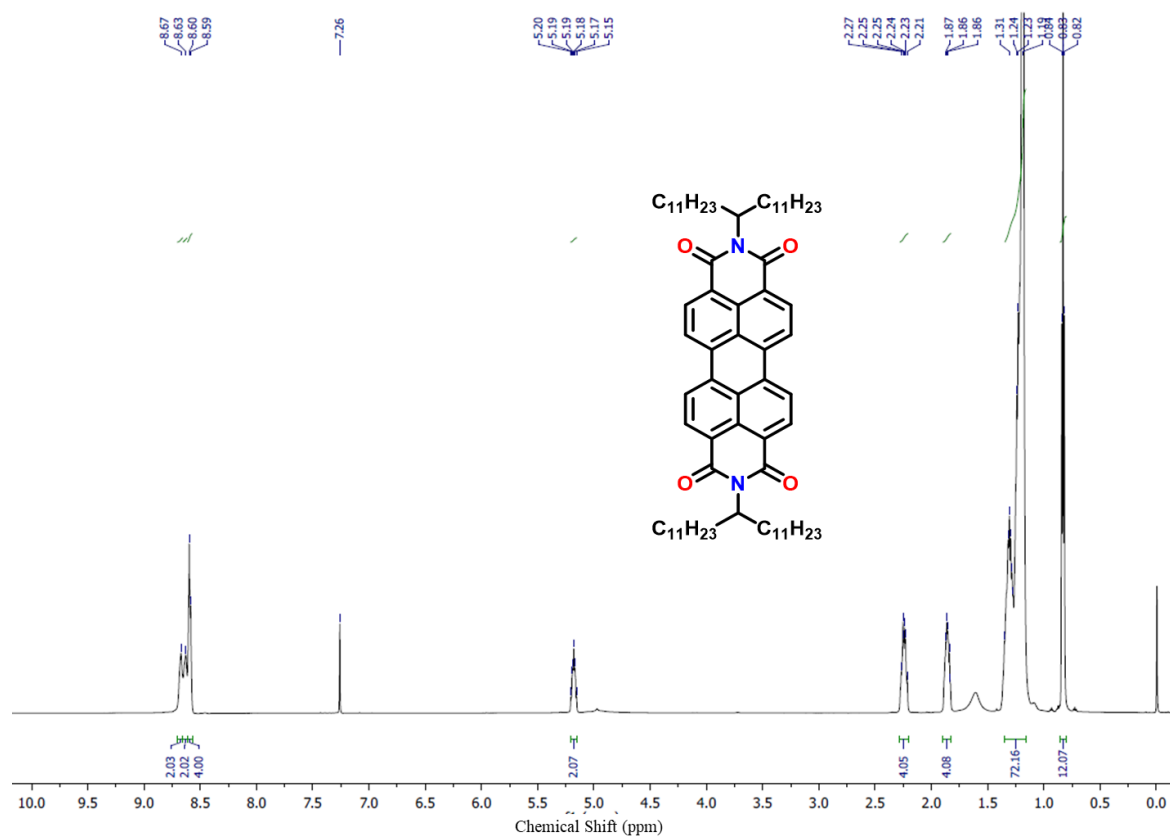


Figure S1. ^1H NMR (600 MHz) spectra of PBI^{ST} in CDCl_3 .

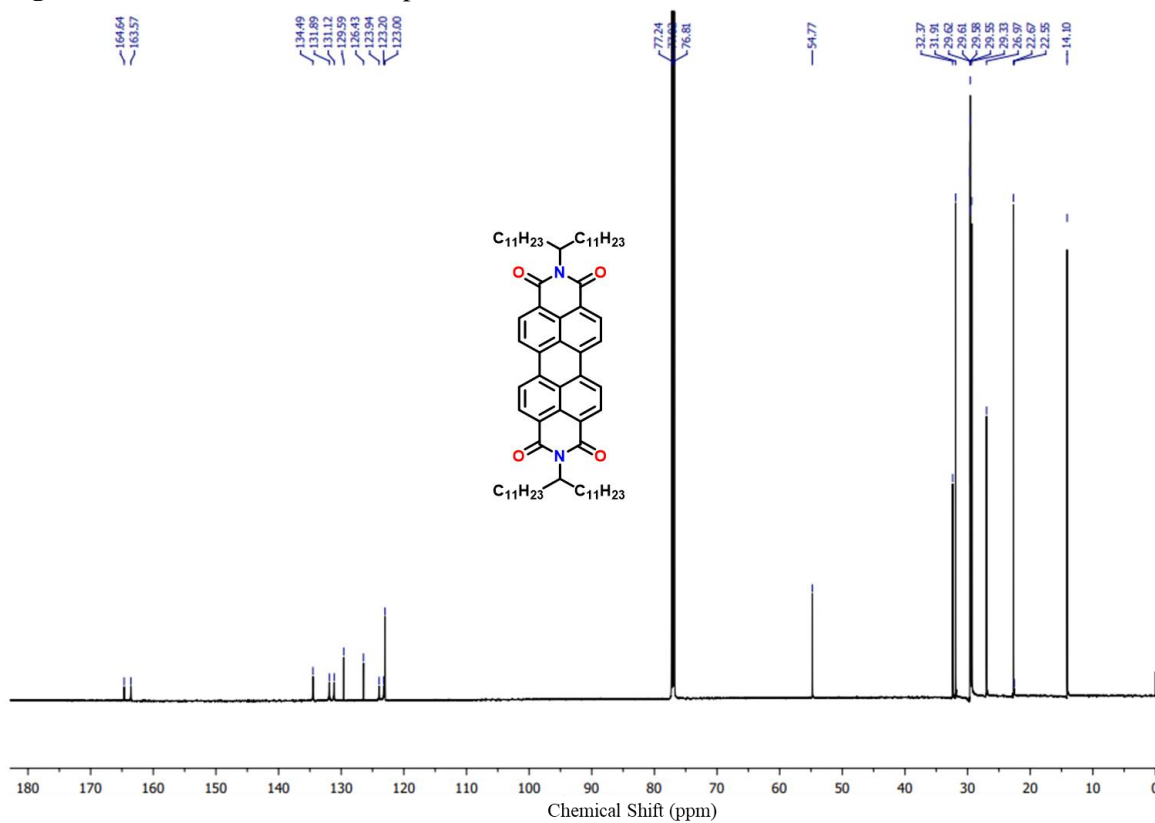


Figure S2. ^{13}C NMR (150 MHz) spectra of PBI^{ST} in CDCl_3 .

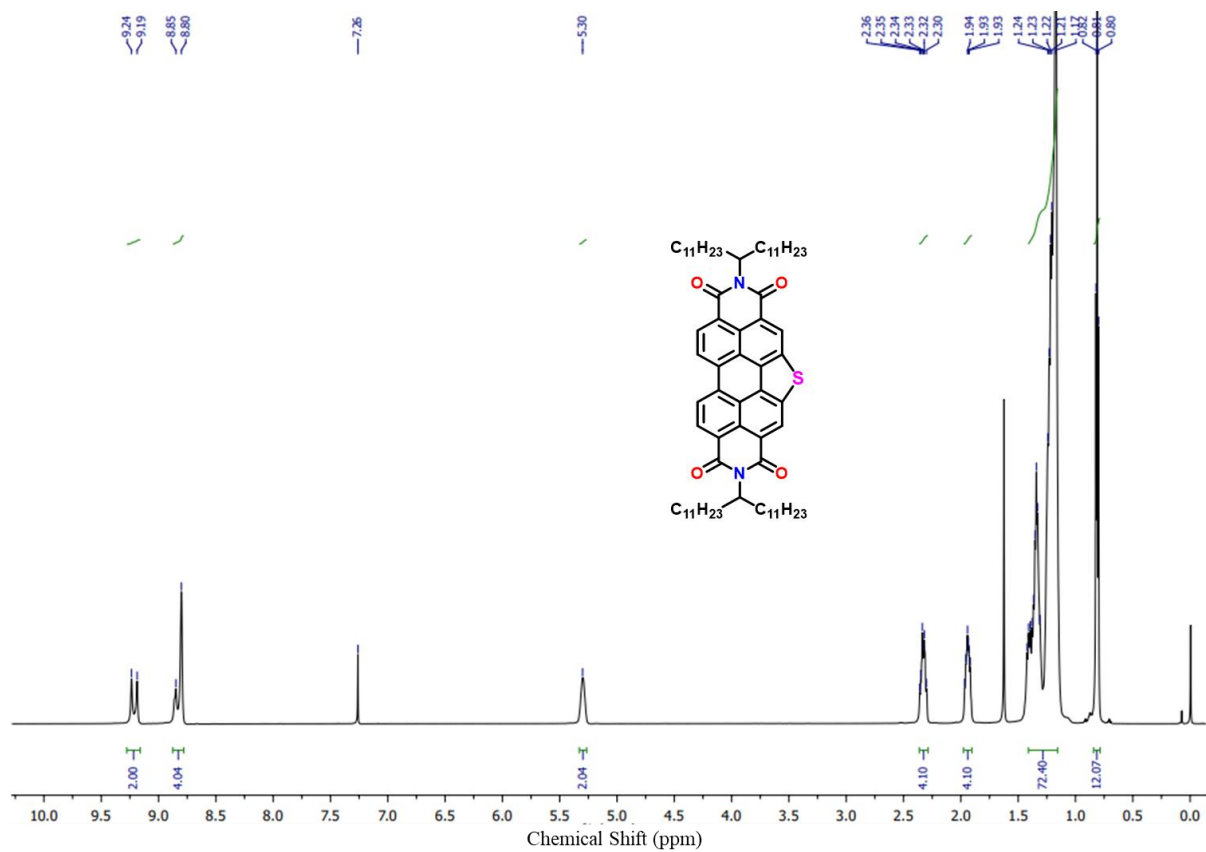


Figure S3. 1H NMR (600 MHz) spectra of **PBI-SST** in $CDCl_3$.

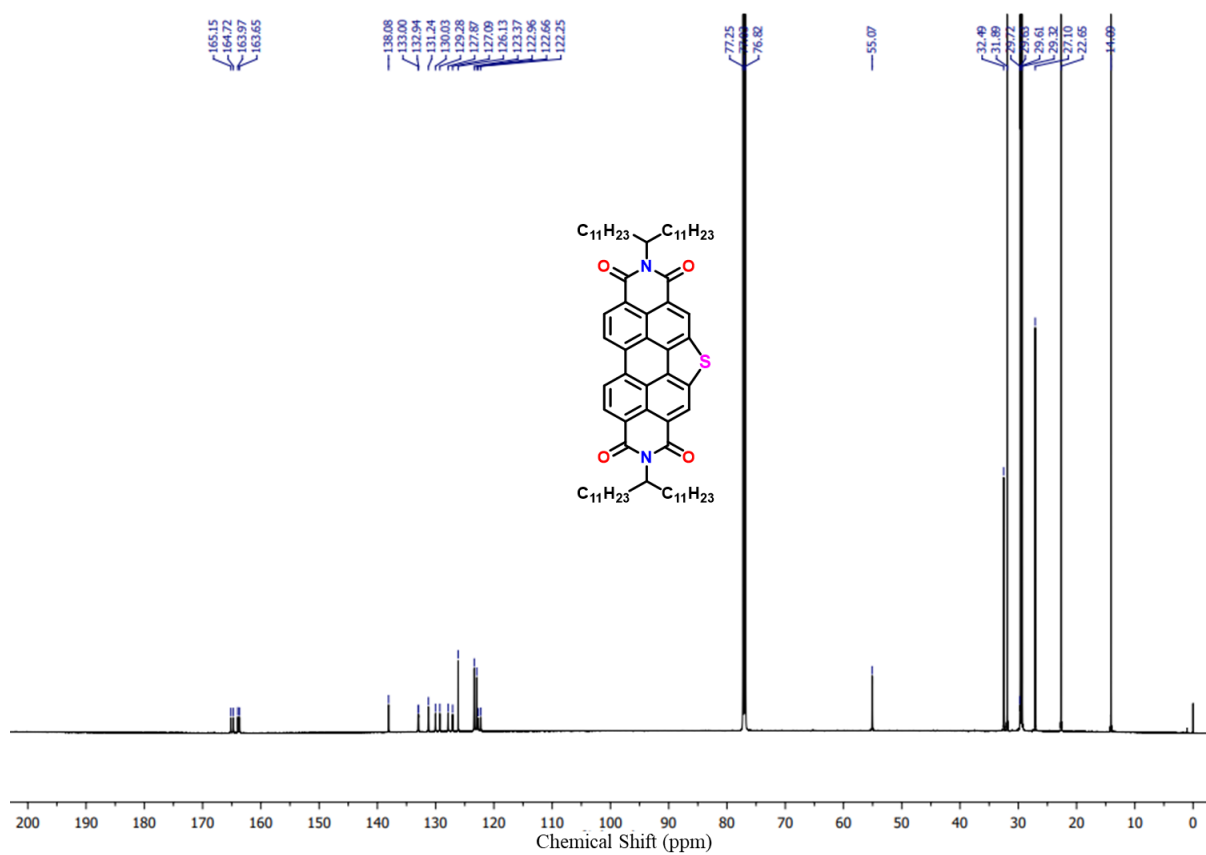


Figure S4. ^{13}C NMR (150 MHz) spectra of **PBI-SST** in $CDCl_3$.

4. MALDI-TOF mass spectra

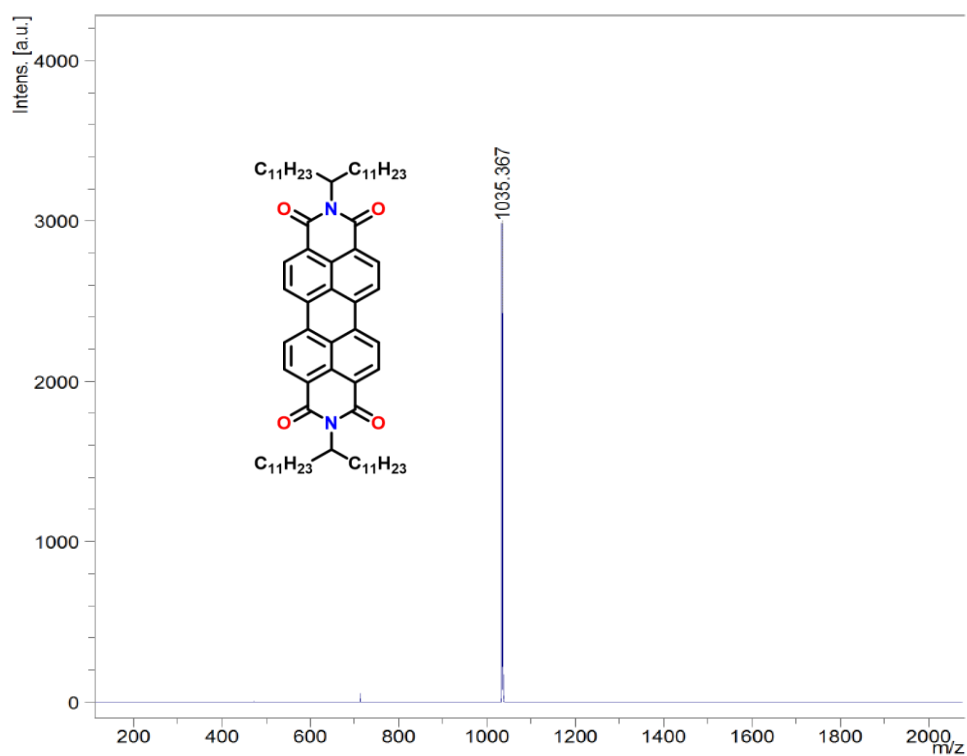


Figure S5. MALDI-TOF mass spectrum of PBIST.

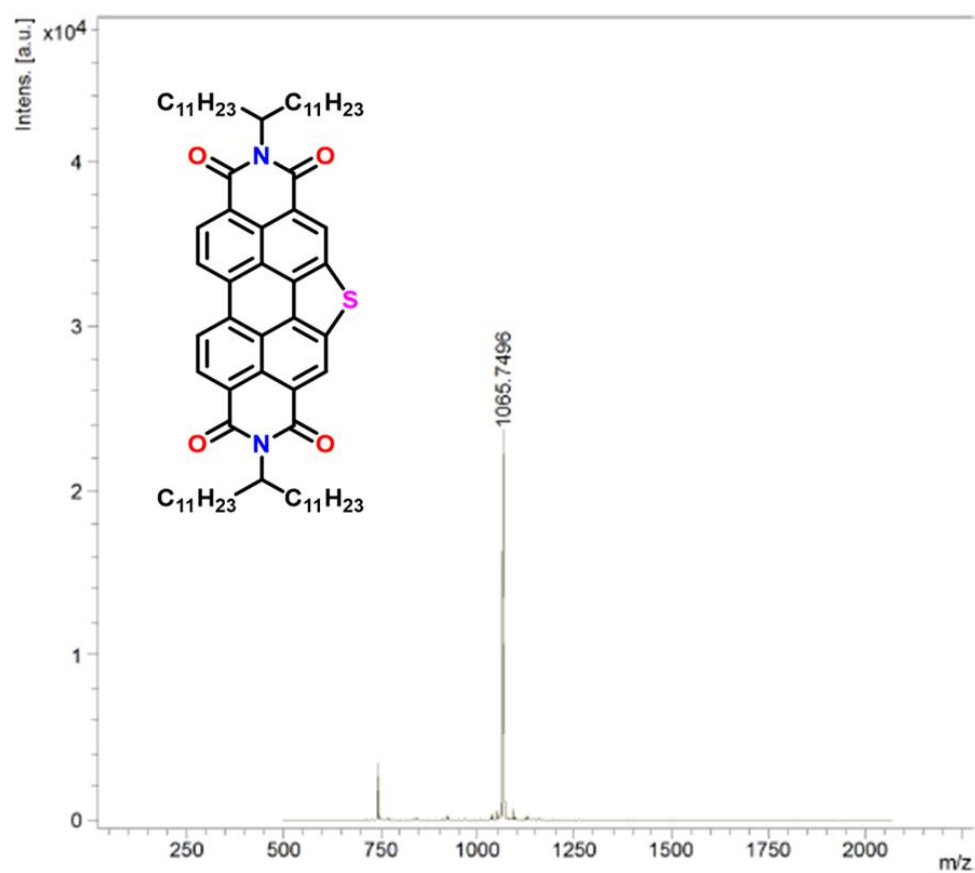


Figure S6. MALDI-TOF mass spectrum of PBI-SST.

5. Thermogravimetric analysis (TGA)

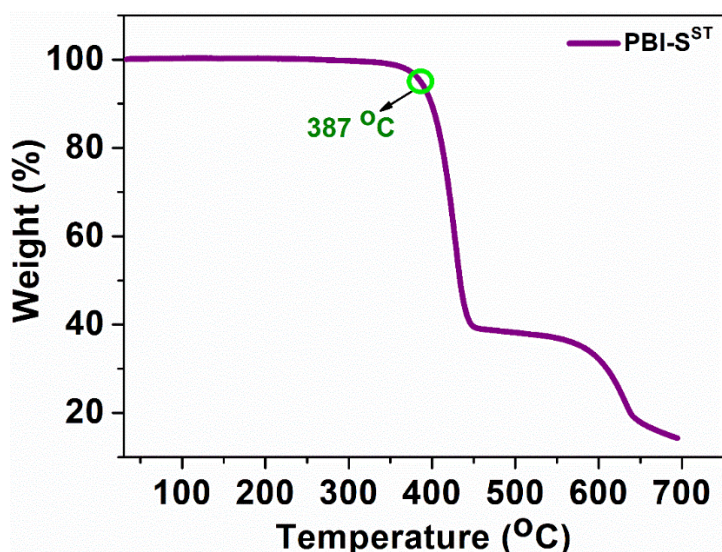


Figure S7. TGA plots of compound PBI-SST (heating rate of 10 °C/min, Nitrogen atmosphere).

6. Differential scanning calorimetry (DSC)

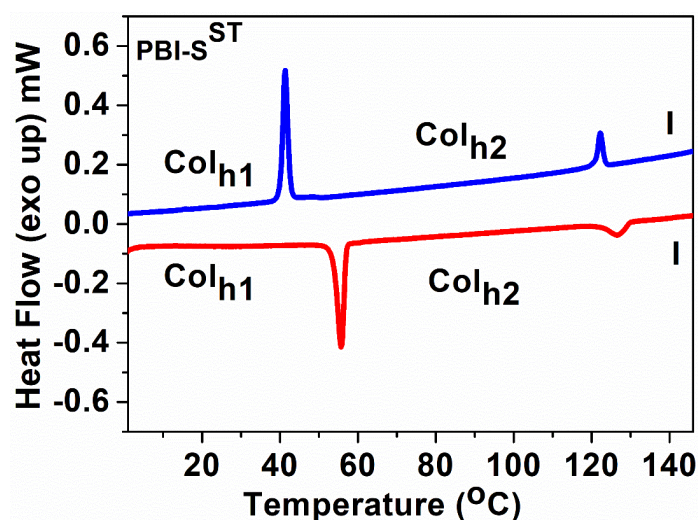


Figure S8. DSC thermogram of PBI-SST at a rate 5 °C/min (Red trace: Second heating scan; Blue trace: First cooling scan).

Table S1. Phase transition temperatures (°C), corresponding enthalpies (kJmol⁻¹)^a and decomposition temperatures obtained for PBI-SST.

Compounds	Phase Sequence (kJ/mol)		T ₅ ^b (°C)
	Second heating	First Cooling	
PBI-S ST	Col _{h1} 56.01 (5.22)	I 122.04 (1.20) Col _{h2}	387
	Col _{h2} 127.16 (0.93) I	41.69 (5.11) Col _{h1}	

^a Peak temperatures in the DSC thermograms obtained during the second heating and first cooling cycles at 5 °C min⁻¹. Col_h = Columnar hexagonal phase; I = Isotropic phase.

7. Polarized Optical Microscopy (POM) Images

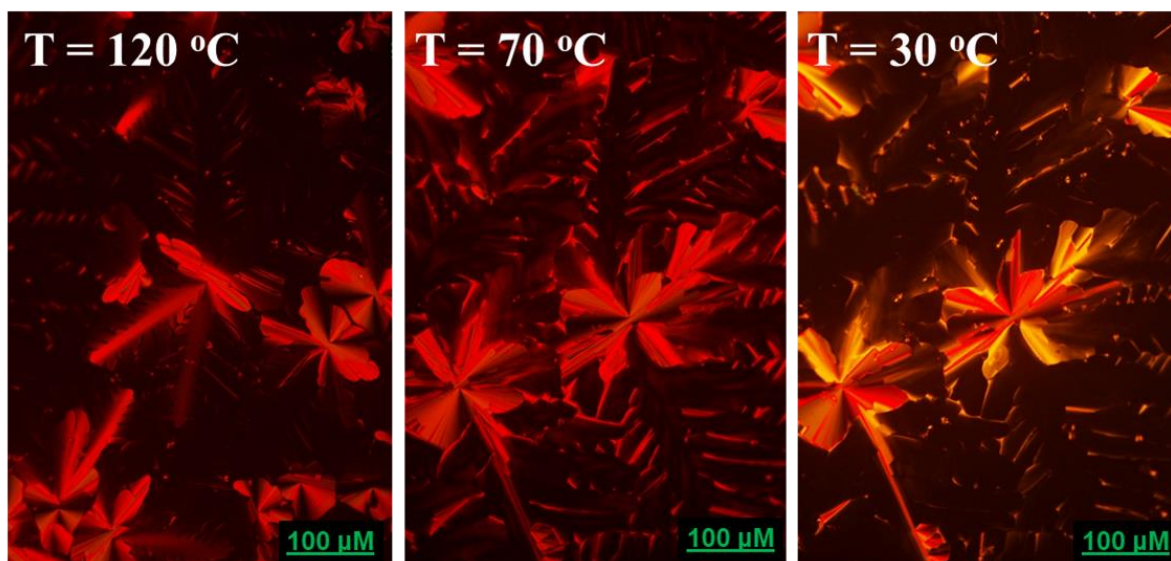


Figure S9. POM images obtained **PBI-SST** at different temperatures (scale bar 100 μm).

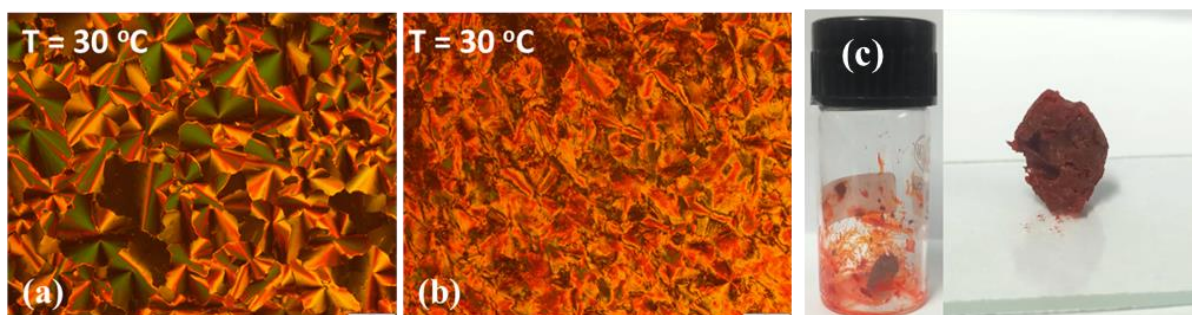


Figure S10. **PBI-SST** in Col_{h1} phase at 30 $^{\circ}\text{C}$ before shearing (a); after shearing (b); Red gummy sticky appearance of **PBI-SST** at room temperature (c).

8. X-ray Diffraction Studies (XRD)

Table S2. Results of (hkl) indexation of XRD profiles of **PBI-SST** at a given temperatures (T) of mesophases^a.

Compounds (D/Å)	Phase (T/ $^{\circ}\text{C}$)	d_{obs} (Å)	d_{cal} (Å)	Miller indices hk	Lattice parameters (Å), Lattice area S (\AA^2), Molecular volume (\AA^3)
PBI-SST (37.86 Å)	Col_h (100)	21.66 12.43 10.74 4.72 (h_a) 3.54 (h_c)	21.66 12.51 10.83	10 11 20	$a = 25.01$ $c = 4.72$ $S = 541.69$ $V = 1917.61$ $Z \approx 1$
	Col_h	21.44 12.31 10.65	21.45 12.38 10.72	10 11 20	$a = 24.76$ $c = 4.64$ $S = 530.92$

MW.:1065.69	(60)	4.64 (h_a) 3.52 (h_c)			$V = 1868.84$ $Z \approx 1$
	Col _h (28)	23.18 13.31 4.83 (h_a) 4.01 (h_c)	23.18 13.38	10 11	$a = 26.77$ $c = 4.83$ $S = 620.60$ $V = 2488.62$ $Z \approx 1$
^a The diameter (D) of the disk (estimated from Chem 3D Pro 22.2.0 molecular model software from Cambridge Soft). d_{obs} : spacing observed; d_{cal} : spacing calculated (deduced from the lattice parameters; a for Col _h phase; c is height of the unit cell). The spacings marked h_a and h_c correspond to diffuse reflections in the wide-angle region arising from correlations between the alkyl chains and core regions, respectively. Z indicates the number of molecules per columnar slice of thickness h_c estimated from the lattice area S and the volume V .					

We have calculated the value of S to determine the value of Z , the number of molecules per unit cell. Regarding calculation of Z , we had used the widely employed formula mentioned below.^{S3}

$$Z = \frac{\rho N_A V_{unit\ cell}}{M}$$

where ρ is the density of the liquid crystal phase, (1 g/cm³)

N_A is Avogadro's constant, (6.022×10^{23})

M is the molecular weight of the constitutive molecule.

V is the Volume of hexagonal unit cell, which is calculated using the formula

$$V_{unit\ cell} = S \times h_c$$

Where h_c is the height of the columnar slice;

S is the lattice area, calculated by the formula,

$$\begin{aligned} S &= a^2 \times \sin 60 \\ &= a^2 \times \sqrt{3}/2 \end{aligned}$$

Where a is hexagonal cell parameter or lattice parameter

$$\begin{aligned} a &= d_{100}/\cos 30 \\ a &= 2/\sqrt{3} \times d_{100} \end{aligned}$$

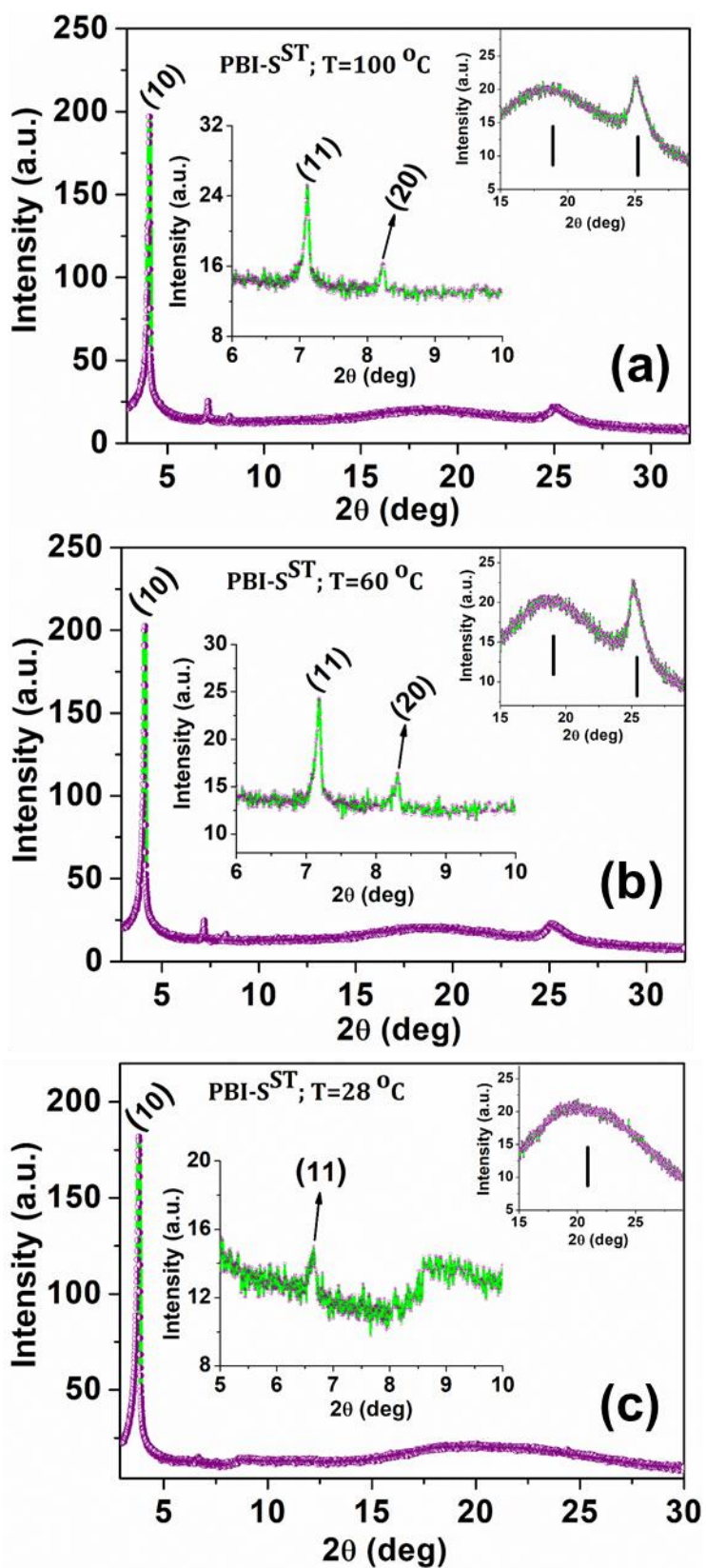


Figure S11. Plot of the intensity against 2θ obtained from the powder XRD pattern of the Col_h phases PBI-S^{ST} at $100\text{ }^\circ\text{C}$ (a); $60\text{ }^\circ\text{C}$ (b); $28\text{ }^\circ\text{C}$ (c).

9. Photophysical studies

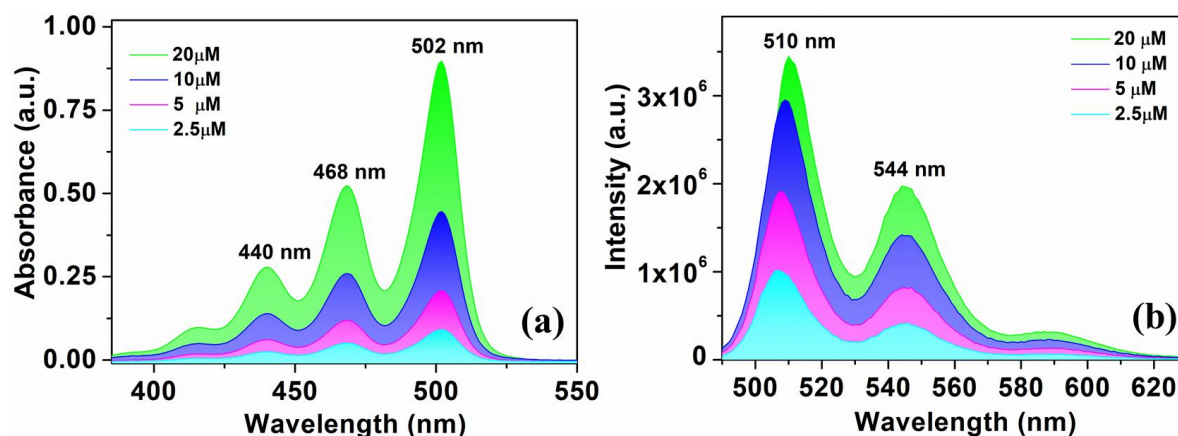


Figure S12. Absorption (a) emission (b) spectra of **PBI-SST** in chloroform solution as a function of concentration.

Table S3. Photophysical properties of **PBI-SST** in solution^a and thin film^b state.

Entry	Absorption [nm]	Emission ^c [nm]	Stokes Shift (cm ⁻¹)	Molar extinction coefficient (ε) (L mol ⁻¹ cm ⁻¹)	Quantum yield ^d (Q _S)	ΔE _{g, opt} ^f [eV]	Absorption [nm]	Emission ^g [nm]	Stokes Shift (cm ⁻¹)
PBI-SST	413, 440, 468, 502	510, 544	313	45,000	0.74 ^d 0.41 ^e	2.40	445, 478, 513	613	4607

^a Micromolar solution in CHCl₃. ^b Prepared by drop casting of millimolar solution in toluene. ^c The excitation wavelength λ_{ex} = 502 nm for **PBI-SST**. ^d Relative quantum yields are calculated with respect to Rhodamine-6G (λ_{ex} = 530 nm) in ethanol solution as the standard and compounds in CHCl₃. ^e Absolute quantum yield in the thin film state. ^f Calculated from the red edge of the absorption band. ^g Excited at the absorption maxima.

10. Quantum yield measurement (Relative)

Quantum yield was measured according to established procedure by using rhodamine 6g in ethanol as the standard. Absolute values were calculated according to the following equation: $Q_S = Q_R \times (m_S / m_R) \times (n_S / n_R)^2$, Where, Q: Quantum yield, m: Slope of the plot of integrated fluorescence intensity vs absorbance (Calculated from Fig.S11), n: refractive index (1.361 for ethanol and 1.445 for chloroform). The subscript R refers to the reference fluorophore i.e. rhodamine 6G solution in EtOH and subscript S refers to the sample under investigation. In order to minimize re-absorption effects, absorbance was kept below 0.15 at the excitation wavelength of 502 nm for compounds **PBI-SST**. Quantum Yield of rhodamine 6g in EtOH is 0.95. Simplified equation for the calculation after substituting the appropriate values is given below and values obtained are given in table below.

$$Q_S = 0.95 \times (m_S / m_R) \times (1.445/1.361)^2$$

Compounds	m _S	m _R	Q _S ^{a,b,c}
PBI-SST	6.37322 × 10 ⁸	9.53557 × 10 ⁸	0.74

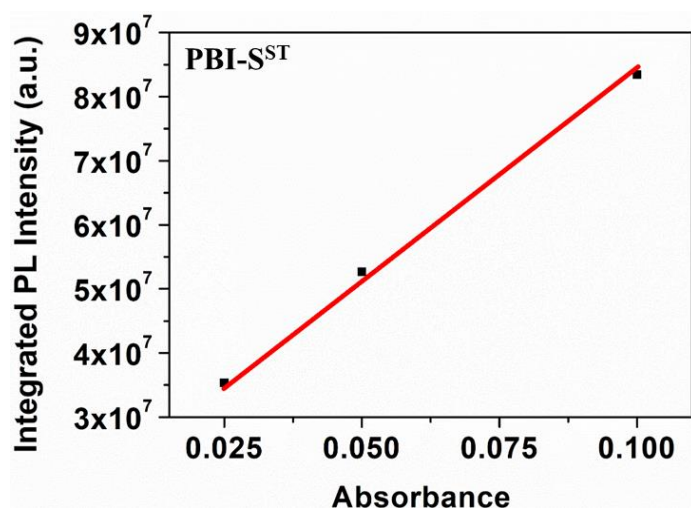


Figure S13. Plots of integrated photoluminescence intensity vs absorbance of compound **PBI-SST**.

11. Cyclic voltammetry (CV)

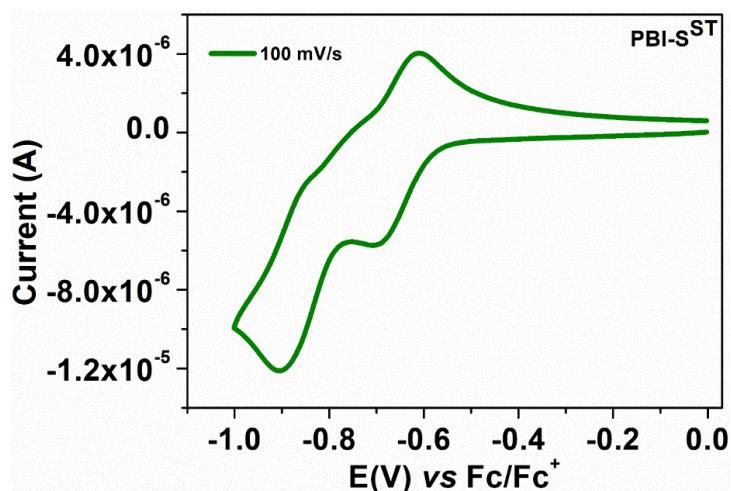


Figure S14. Cyclic voltammograms of **PBI-SST**.

Table S4. Electrochemical^{a,b} data and data obtained from DFT^h calculations for compounds **PBI-SST**.

Entry	Electrochemical data				Data from DFT calculations		
	$E_{1st\ red}^{[c]}$	$E_{LUMO}^{[d,e]}$	$E_{HOMO}^{[d,f]}$	$\Delta E_{g,\ opt}^{[d,g]}$	$E_{LUMO}^{[d,h]}$	$E_{HOMO}^{[d,h]}$	$\Delta E_{g,\ }^{[d,h]}$
PBI-SST	-0.70	-3.57	-5.97	2.40	-3.39	-6.09	2.70

^[a]0.5 mM Dichloromethane solutions; ^[b]experimental conditions: Ag/AgNO₃ as reference electrode, glassy carbon working electrode, platinum wire counter electrode, TBAP (0.1M) as a supporting electrolyte, room temperature; ^[c] in volts (V); ^[d] in eV; ^[e] estimated from the formula by using $E_{LUMO} = -(4.8 - E_{1/2, Fc/Fc^+} + E_{red, onset})$ eV; ^[f] estimated from the formula $E_{HOMO} = (E_{LUMO} - E_{g,\ opt})$ eV; $E_{1/2, Fc/Fc^+} = 0.50$ V. ^[g]calculated from the red edge of the absorption band of each compound. ^[h] Obtained from DFT calculations by employing the combination of Becke3-Lee-Yang-Parr (B3LYP) hybrid functional and 6-31G(d,p) basis set using the Gaussian 09 package.

12. Device Fabrication and Characterizations

Based on superior photophysical and electrochemical properties, the electroluminescent properties of **PBI-SST** emitter material, was investigated. Multi-layered solution processed OLED was fabricated consisting of following device configurations: anode: ITO (125 nm)/HIL: PEDOT:PSS (40 nm)/ EML (20 nm)/ ETL: TPBi (35 nm)/EIL: LiF (1 nm)/cathode: Al (100 nm). Initially, ITO-coated glass substrates were cleaned to remove greasy layer. The cleaning process was carried-out with soap-solution, deionized water, acetone, and alcohol in water-bath sonicator at optimized time. Cleaned substrates were kept in ultra-violet ozone system to expose in UV-light for removing residual solvents and further impurities. Then, these substrates were transferred into nitrogen purged glovebox for further processing of layers. Simultaneously, CBP as host and newly synthesized emitter (**PBI-SST**) for emissive solution layer was dispersed into suitable solvents with water-bath sonicator. Prepared solution was filtered with 0.45 μm PTFE filters and mixed in desired ratio to prepare emissive layer. First, a hole-injection layer was prepared by spin-coating an aqueous solution of PEDOT:PSS at 4,000 rpm for 20 s. Subsequently, these substrates were annealed at 130 °C for 15 minutes. After cooled down the substrates, neat solution or emissive layer solution was spin-coated onto hole-injection layer at 2,500 rpm for 20 s. Then, these substrates were transferred into thermal evaporator to deposit subsequent layers. Then, TPBi was deposited as an electron-transport layer followed by the deposition of 0.5 nm LiF as an electron-injection layer and 100 nm Al as a cathode. All the layers of TPBi, LiF and Al were deposited subsequently via thermal evaporation method at base pressure of 4.0×10^{-6} Torr. After that, Fabricated devices were kept in the mini vacuum chamber during testing process and then measured at room temperature conditions. To analyse the device, the electroluminescence (EL) spectrum, luminance, and the CIE coordinates were obtained using a photo research (PR-655) spectrometer. The current density-voltage-luminance (J-V-L) characteristics were obtained by a computer mounted voltmeter (Keithley 2400) and spectrophotometer CS-100 Minolta.

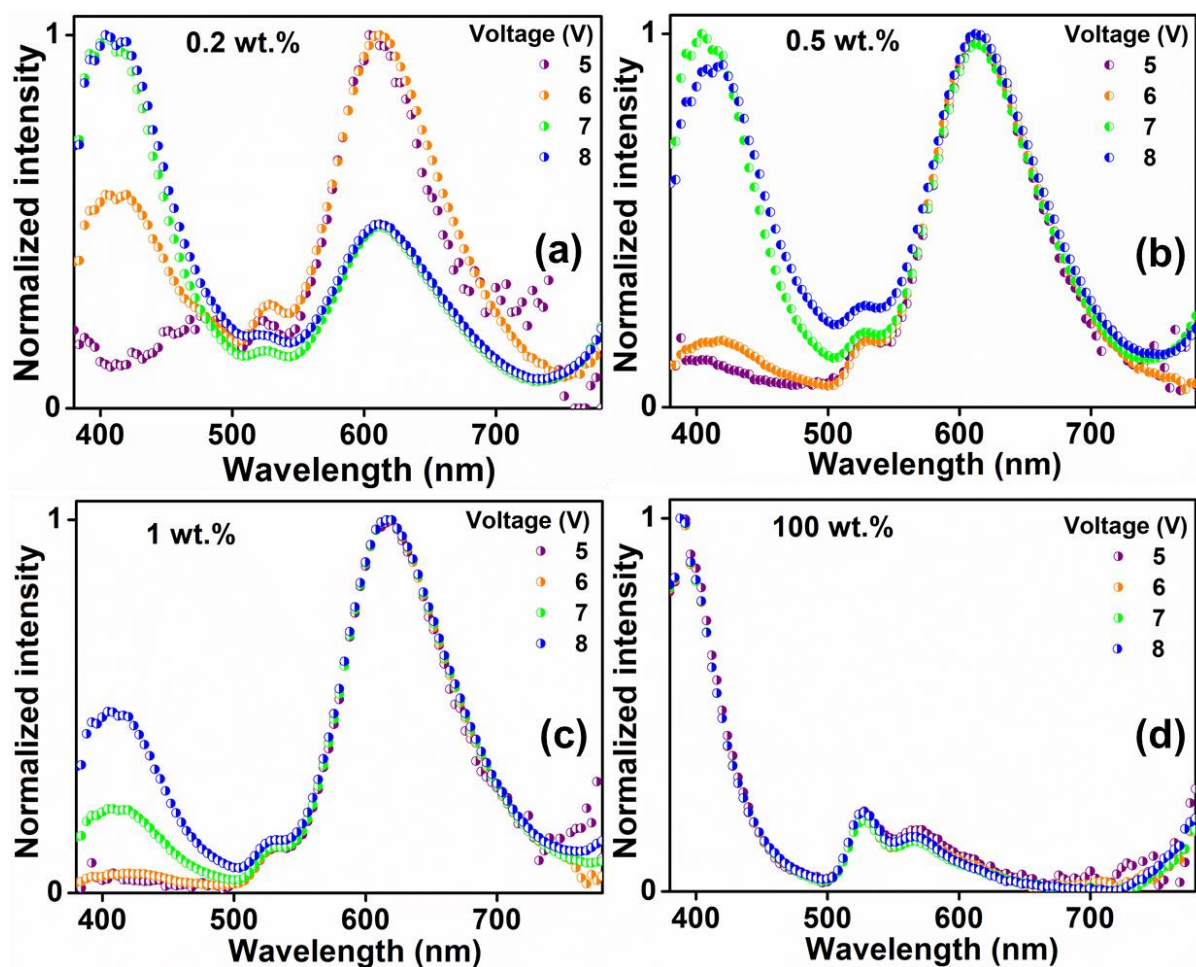


Figure S15. The electroluminescent spectra of PBI-SST at a varying voltage of the doped devices at varying concentrations (a) 0.2, (b) 0.5 and (c) 1.0 wt% in the CBP host matrix, along with the (d) undoped (100 wt%) device.

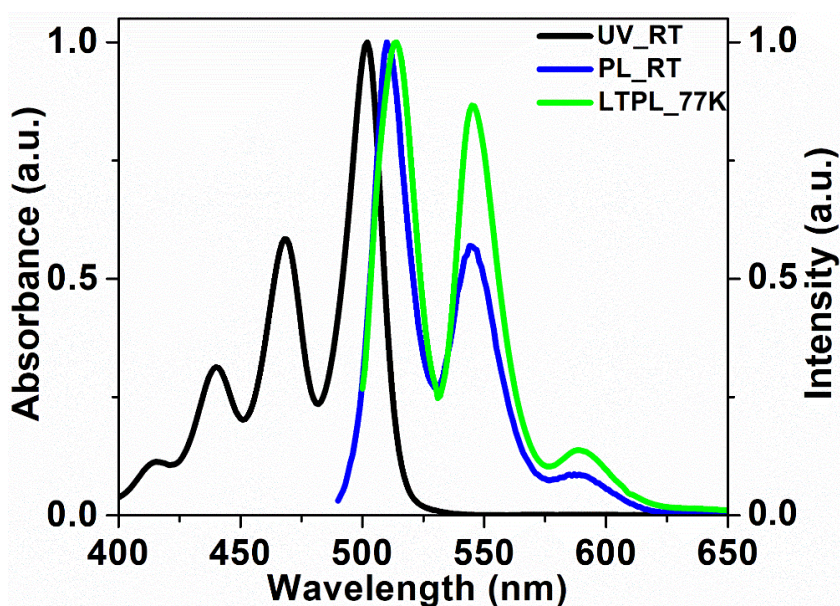


Figure S16. Overlay of absorbance, photoluminescence, low temperature photoluminescence spectra of PBI-SST in solution state.

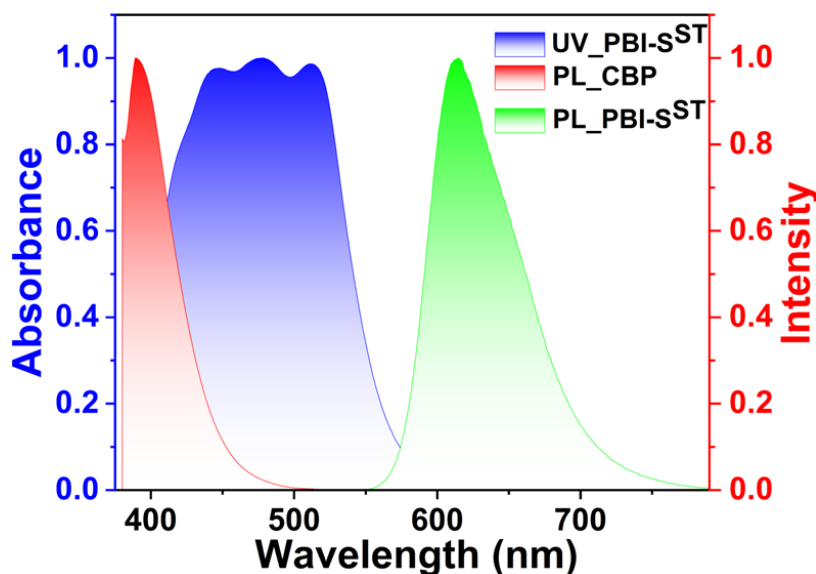


Figure S17. Overlay of absorbance and emission spectra of **PBI-SST** and photoluminescence spectra of **CBP** in thin film state

Table S5. Solid state PLQY values of **PBI-SST** and in its doped state with CBP at 0.5 wt%.

Compound	PLQY
PBI-SST (0.5 wt%)	79 %
PBI-SST (100 wt%)	41 %

13. Surface Morphology Studies (AFM)

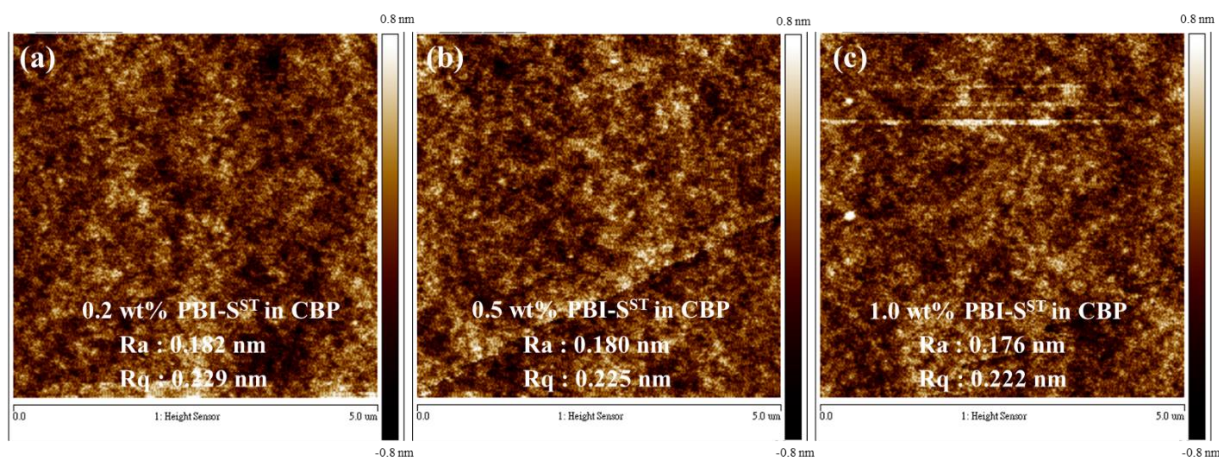


Figure S18. AFM images or the surface morphologies of 0.2 wt% (a), 0.5 wt% (b), and 1.0 wt% (c) of **PBI-SST** emitter doped in CBP host matrix.

14. DFT Studies

To understand the electronic properties and frontier molecular orbital energy level of compounds **PBI-SST** computational studies was carried out in B3LYP/6-31g(d,p) method using Gaussian 09 program package.^{S4} The absence of imaginary frequency ensured the energy minimized structure of all the compounds.

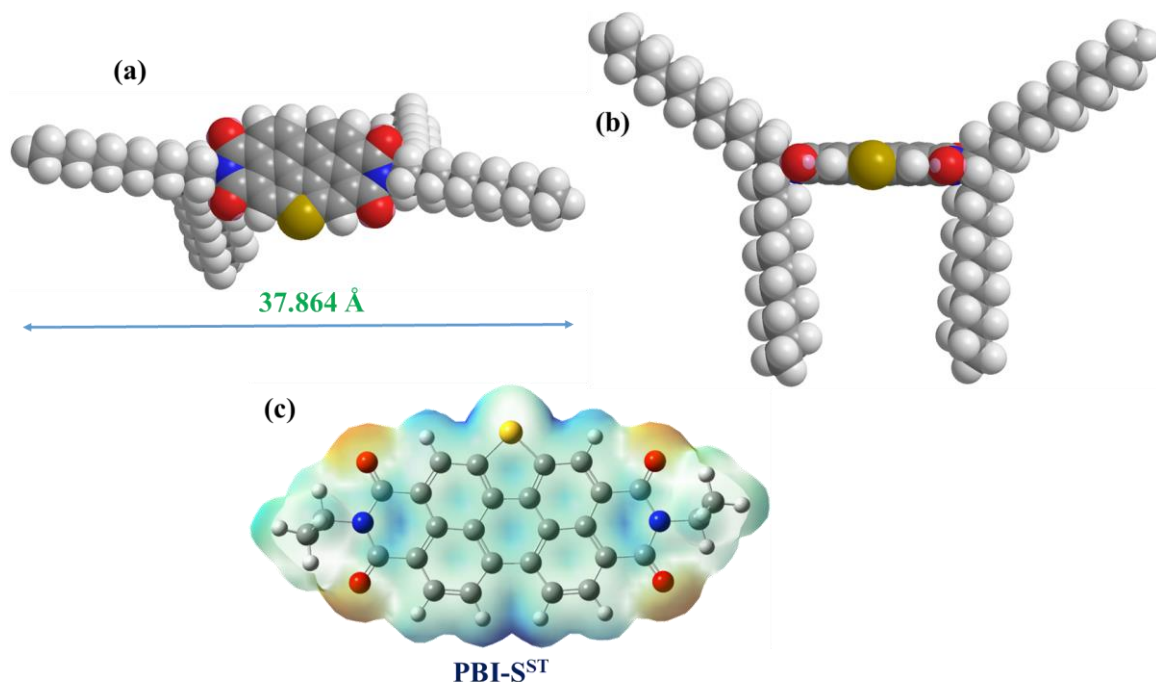


Figure S19. Energy minimized molecular model of **PBI-SST** (a) top view; (b) side view; (c) 3D molecular electrostatic potential contour map of optimized structure of **PBI-SST** (In the mapped electrostatic potential surface, the red and blue colors refer to the electron-rich and electron-poor regions, respectively, whereas the green color signifies the zero electrostatic potential, chain length is limited to methyl for clarity purpose).

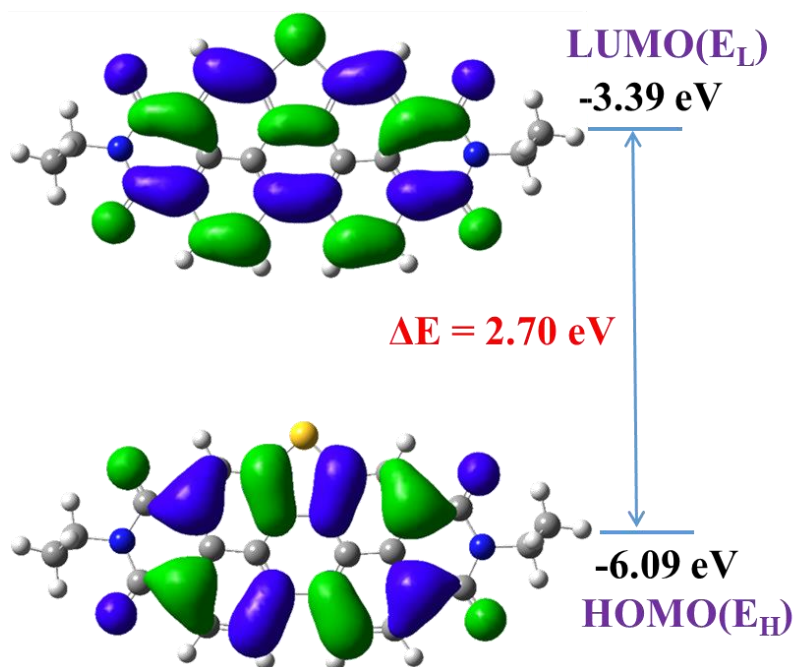


Figure S20. Frontier molecular orbitals of **PBI-SST** obtained from tricosan-12-amine. DFT calculations at the B3LYP/6-31G(dp) level. E_H and E_L denote energies of the highest occupied molecular orbital (HOMO) and the lowest unoccupied molecular orbital (LUMO), respectively (chain length is limited to methyl for clarity purpose).

DFT calculation data for PBI-SST:

Center Number	Atomic Number	Atomic Type	Coordinates (Angstroms)		
			X	Y	Z
1	6	0	2.765672	2.717958	-0.001709
2	6	0	1.404994	2.771360	-0.002433
3	6	0	0.645846	1.635339	-0.002380
4	6	0	1.381030	0.472502	-0.001850
5	6	0	2.745948	0.371181	-0.001220
6	6	0	3.453551	1.537619	-0.000958
7	6	0	0.703166	-0.695977	-0.001984
8	6	0	1.229062	-1.946722	-0.001871
9	6	0	2.593397	-2.018183	-0.001480
10	6	0	3.342620	-0.870794	-0.001051
11	6	0	-0.747196	1.586081	-0.002556
12	6	0	-1.398337	0.374168	-0.002214
13	6	0	-0.639548	-0.743419	-0.002143
14	6	0	-1.584320	2.666043	-0.003038
15	6	0	-2.937798	2.516684	-0.002855
16	6	0	-3.539615	1.290479	-0.002122
17	6	0	-2.752576	0.176185	-0.001736
18	6	0	-3.261393	-1.104449	-0.001403
19	6	0	-2.432032	-2.195490	-0.001785
20	6	0	-1.076111	-2.028030	-0.001982
21	6	0	4.736028	-0.955666	-0.000314
22	7	0	5.446873	0.249225	0.002212
23	6	0	4.846937	1.514942	0.000071
24	6	0	-4.927459	1.169003	-0.001490
25	7	0	-5.438769	-0.132320	0.002602
26	6	0	-4.645741	-1.288062	-0.000560
27	8	0	5.511269	2.537397	-0.000672
28	8	0	5.319240	-2.025967	-0.001731
29	8	0	-5.665011	2.138977	-0.004218
30	8	0	-5.148185	-2.399387	-0.002022
31	6	0	6.927160	0.183484	0.006556
32	6	0	-6.911008	-0.299645	0.008825
33	6	0	7.507155	-0.443451	1.287143
34	6	0	7.513950	-0.431546	-1.276657
35	6	0	-7.580713	0.234142	1.288003
36	6	0	-7.586719	0.213223	-1.275383
37	6	0	0.112273	-3.000744	-0.002104
38	1	0	3.295367	3.680439	-0.001771
39	1	0	0.949308	3.769542	-0.002974
40	1	0	3.056350	-3.014371	-0.001198
41	1	0	-1.200308	3.693882	-0.003416
42	1	0	-3.535325	3.438699	-0.003186
43	1	0	-2.821907	-3.222425	-0.001498
44	1	0	7.354561	1.209948	0.013433
45	1	0	-7.174164	-1.379835	0.020181
46	1	0	8.607812	-0.307720	1.328984
47	1	0	7.075804	0.037909	2.189399
48	1	0	7.321806	-1.531363	1.364565
49	1	0	8.615348	-0.299749	-1.309159
50	1	0	7.091042	0.061496	-2.176504
51	1	0	7.323972	-1.517686	-1.366979
52	1	0	-8.646587	-0.071533	1.331955
53	1	0	-7.078871	-0.170449	2.191451
54	1	0	-7.567385	1.337988	1.360970
55	1	0	-8.654748	-0.086473	-1.305952

56	1	0	-7.093679	-0.211999	-2.174246
57	1	0	-7.565714	1.315370	-1.369486

15. TD-DFT and NTO calculations:

Excited states were calculated by time-dependent DFT (TD-DFT) calculations the using the ground state optimized geometries.

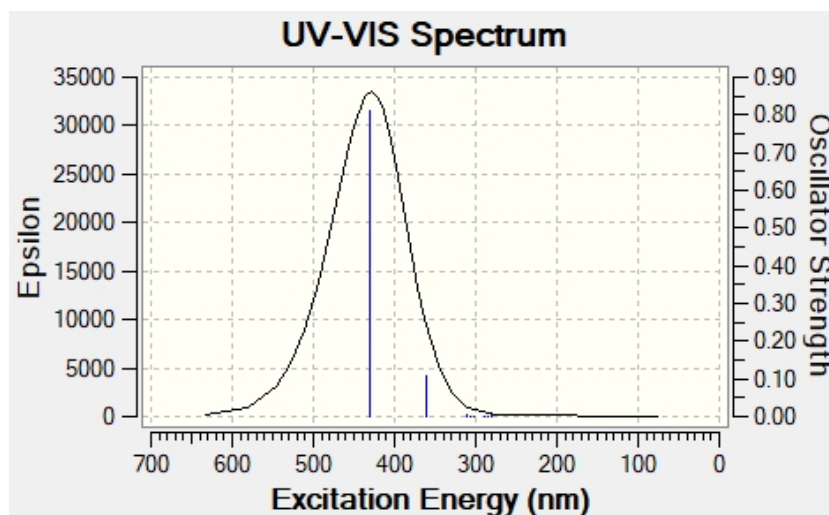
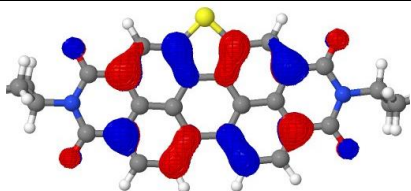
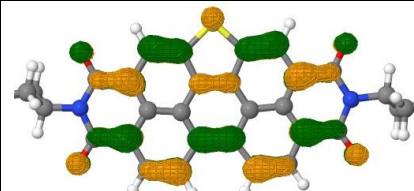


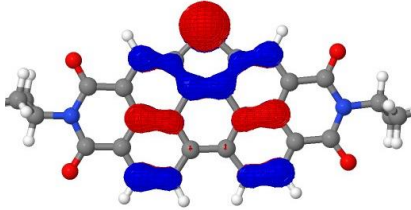
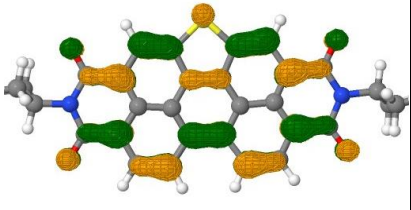
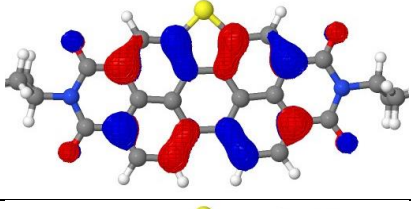
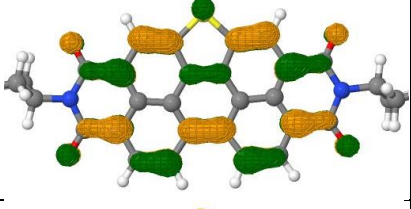
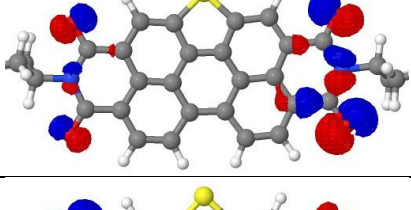
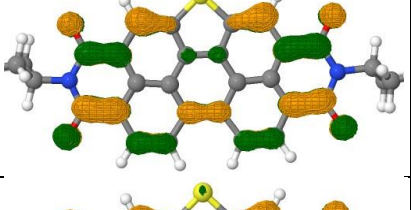
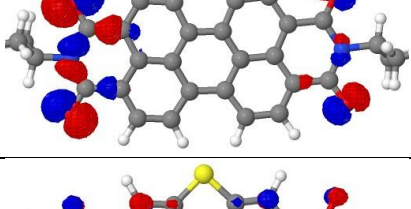
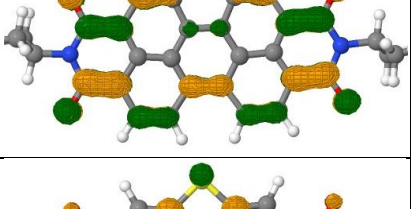
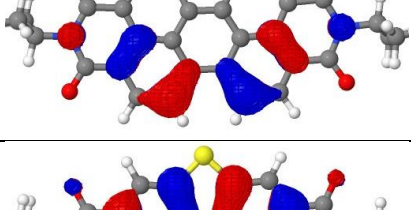
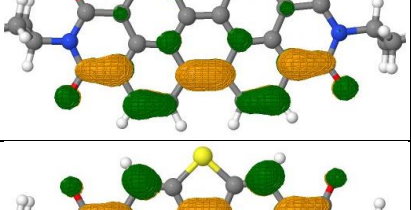
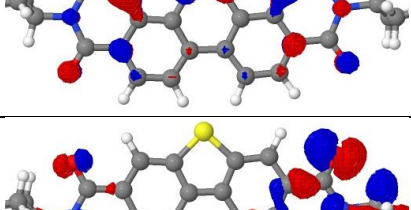
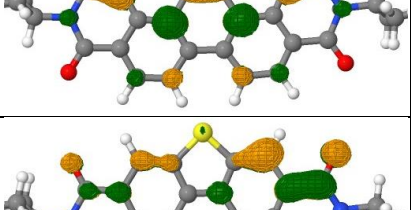
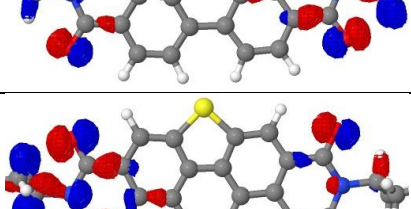
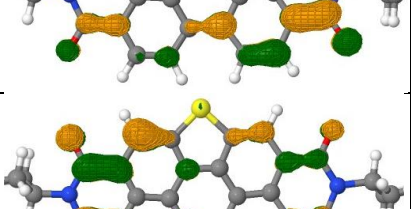
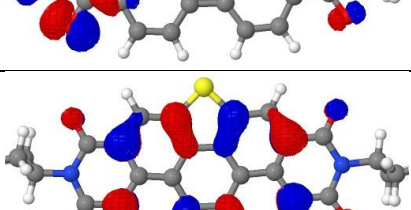
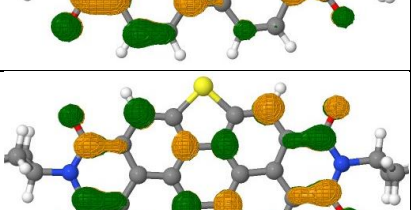
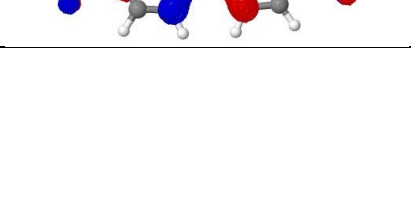
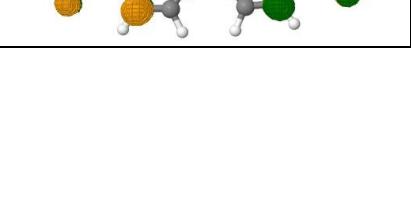
Figure S21. TD-DFT simulated UV-vis absorption spectra of compound **PBI-SST** (no. of states considered =40).

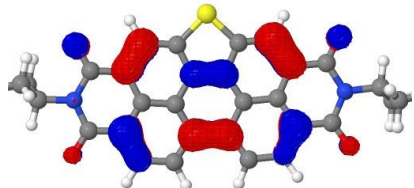
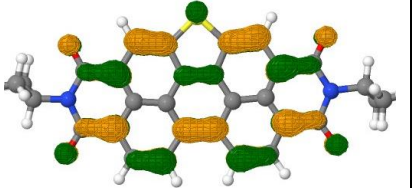
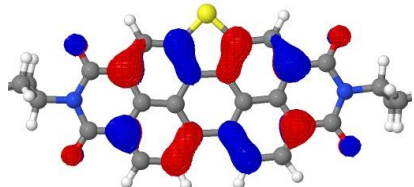
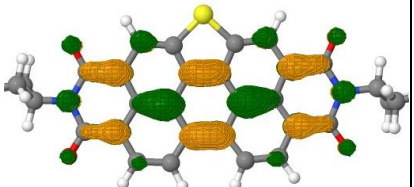
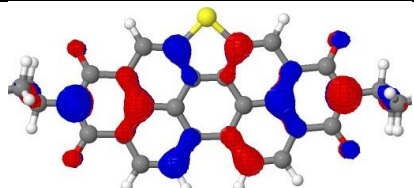
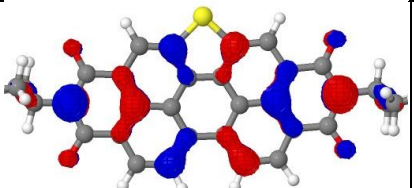
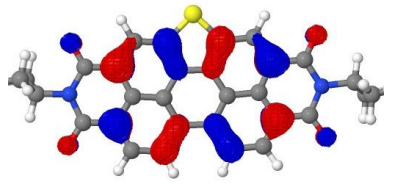
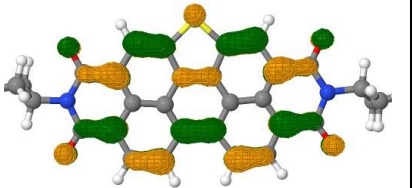
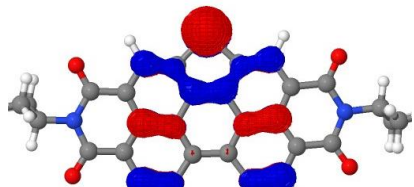
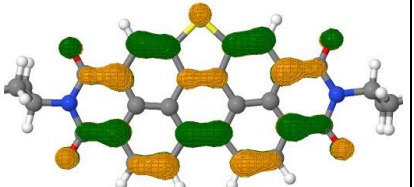
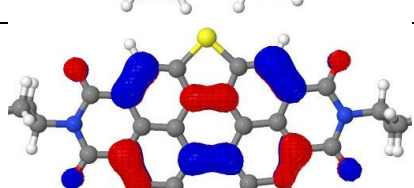
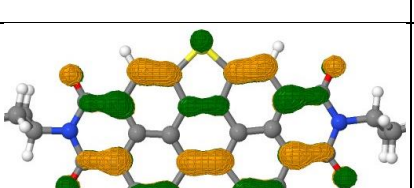
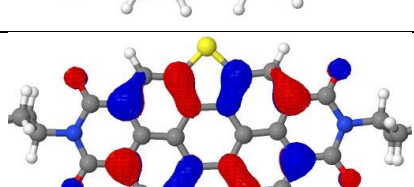
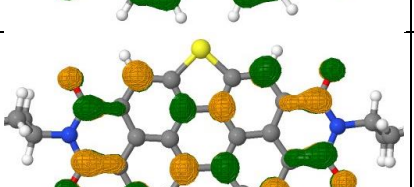
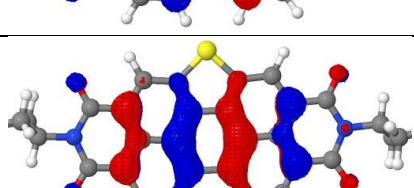
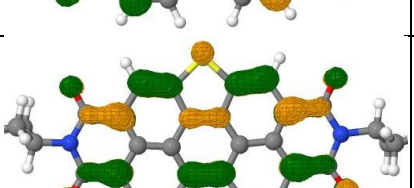
The singlet energy (E_S) of material **PBI-SST** calculated from the fluorescence spectra (at room temperature) is found to be 2.45 eV (calculated from emission maxima (recorded in THF)) while $E_S = 2.88$ eV has been estimated from TD-DFT calculation.

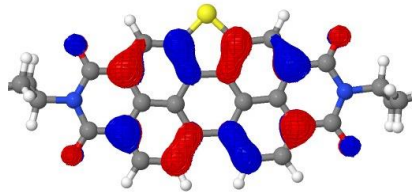
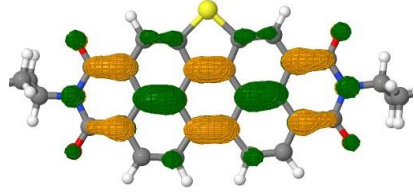
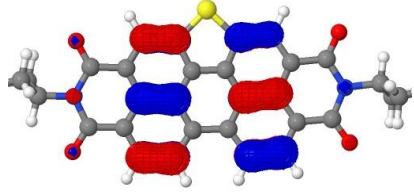
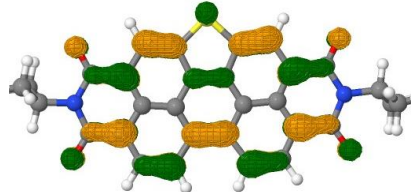
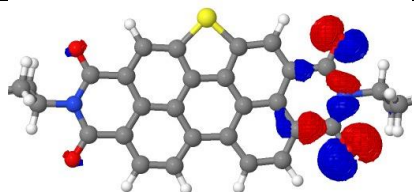
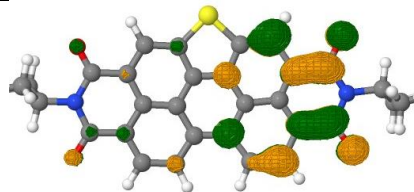
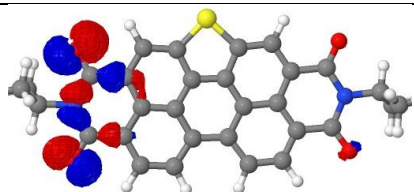
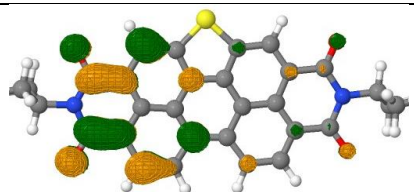
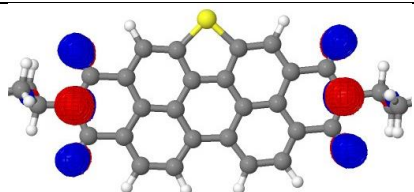
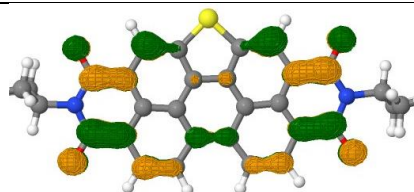
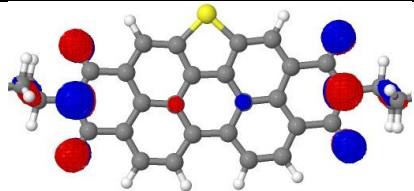
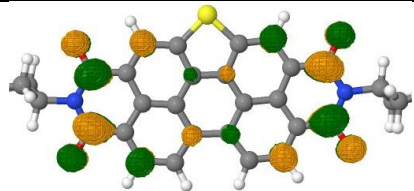
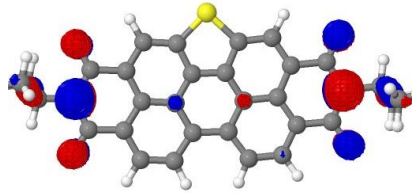
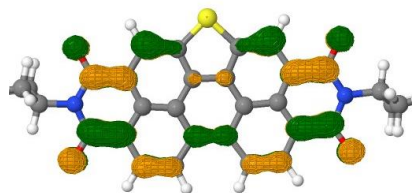
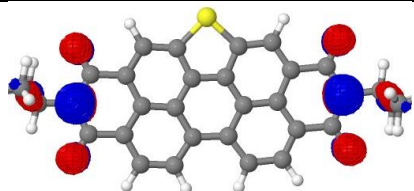
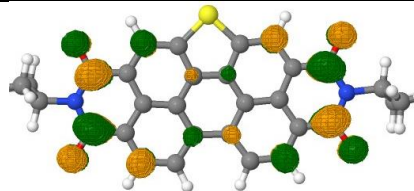
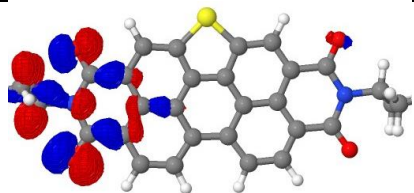
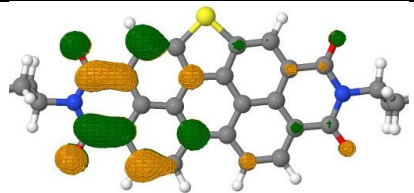
No phosphorescent spectrum of **PBI-SST** is observed (Figure S16) (as performed in THF at 77 K) which is indicative of low density of the T_1 state in **PBI-SST**. The similar fact has been reported in the literature.^{S5} While from TD-DFT the calculated triplet energy of the T_1 state is $E_T = 1.28$ eV.

Table S6. Calculated natural transition orbitals (NTO) of singlet and triplet excited states.

Excited states (Energies)	Hole	Contribution	Particle	Contribution
S ₁ (2.883 eV)		0.98		0.98

S₂ (3.436 eV)		0.90		0.90
S₃ (3.994 eV)		0.87		0.87
S₄ (4.045 eV)		0.74		0.74
S₅ (4.050 eV)		0.74		0.74
S₆ (4.106 eV)		0.49		0.49
		0.43		0.43
S₇ (4.277 eV)		0.74		0.74
S₈ (4.281 eV)		0.74		0.74
S₉ (4.342 eV)		0.76		0.76

		0.20		0.20
S₁₀ (4.437 eV)		0.55		0.55
		0.39		0.39
Excited states (Energies)	Hole	Contri bution	Particle	Contri bution
T₁ (1.283 eV)		0.96		0.96
T₂ (2.756 eV)		0.94		0.94
T₃ (2.771 eV)		0.47		0.47
		0.41		0.41
T₄ (2.946 eV)		0.48		0.48

		0.42		0.42
T₅ (3.455 eV)		0.76		0.76
T₆ (3.692 eV)		0.85		0.85
T₇ (3.699 eV)		0.84		0.84
T₈ (3.731 eV)		0.61		0.61
		0.24		0.24
T₉ (3.787 eV)		0.71		0.71
		0.23		0.23
T₁₀ (3.931 eV)		0.80		0.80

16. Electron-hole correlation plots for the individual states:

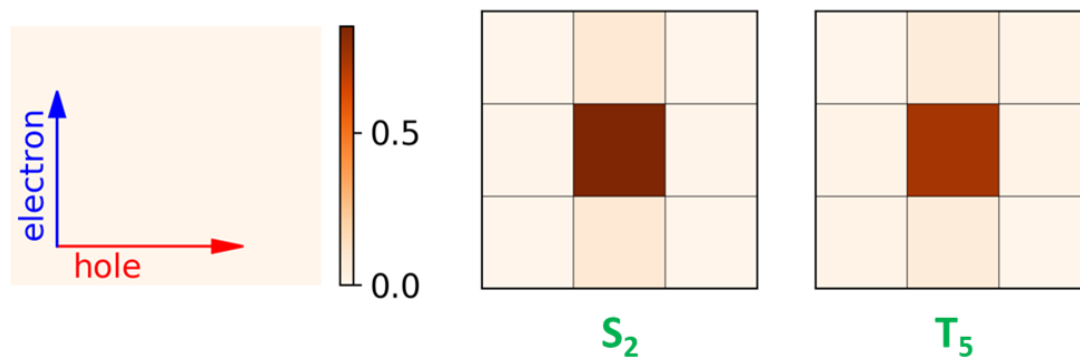


Figure S22. Electron-hole correlation plots of S_2 and T_5 states of compound **PBI-SST**.

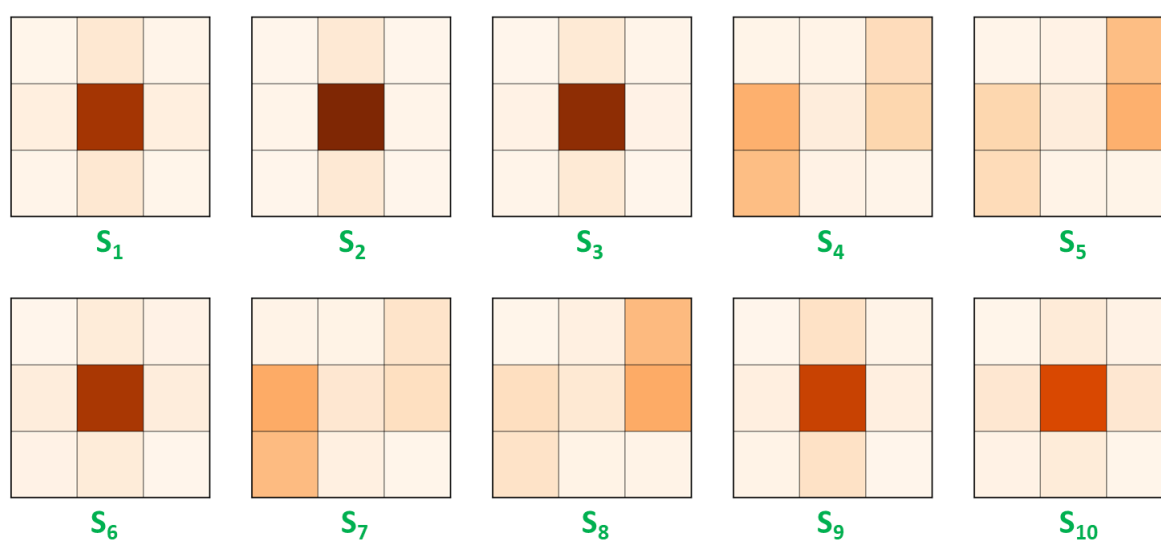


Figure S23. Electron-hole correlation plots of S_1 - S_{10} states of compound **PBI-SST**.

From the above figure it is clear that $S_1, S_2, S_3, S_6, S_9,$ and S_{10} are local excited states with very less charge transfer characteristics while $S_4, S_5, S_7,$ and S_8 shows a dominant charge transfer characteristic.

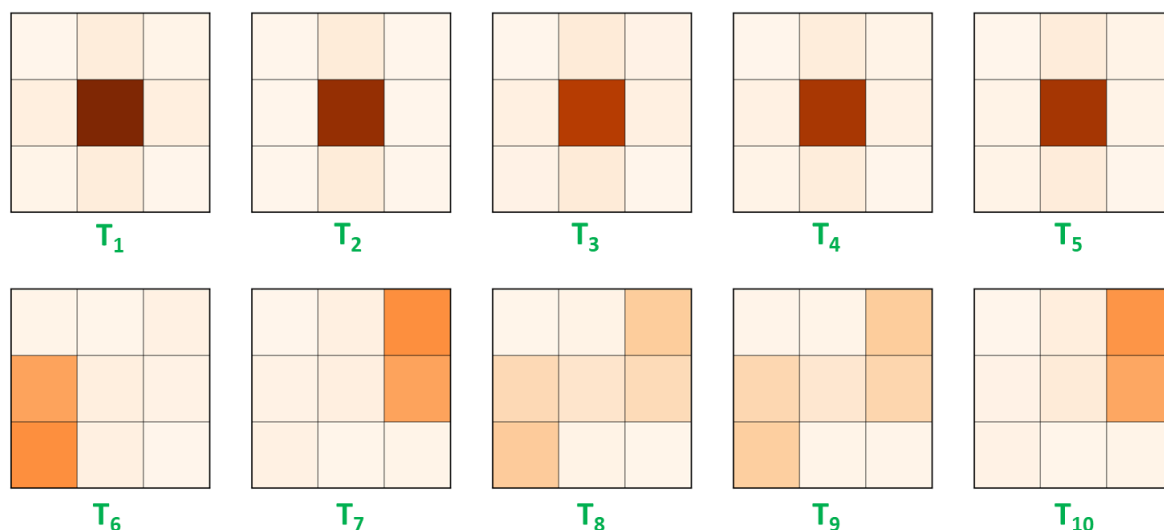


Figure S24. Electron-hole correlation plots of T_1 - T_{10} states of compound **PBI-SST**.

From the above figure it is clear that T_1 , T_2 , T_3 , T_4 , and T_5 are local excited states with very less charge transfer characteristics while T_6 , T_7 , T_8 , T_9 and T_{10} shows a dominant charge transfer characteristics.

17. Solvatochromism

To further investigate the HLCT character of **PBI-SST** we examined its solvatochromism behavior. This involved measuring the absorption (Fig. S25a) and emission (Fig. S25b) spectra in a diverse range of solvents, spanning from non-polar to polar solvents as depicted in Figure S25. It is crucial to note that during our experimental investigations, we encountered challenges in measuring emission spectra in highly polar solvents such as ethanol, DMF, DMSO, methanol, acetone, water, and acetonitrile, as **PBI-SST** exhibited insolubility in these mediums. Despite these challenges, **PBI-SST** exhibited a complex solvatochromic behavior, consistent with existing literature reports.^{S6} From the above experiments we observed a red shift in both absorption and emission spectra with increase in solvent polarity from hexane to chloroform. This shift strongly implies the presence of a charge transfer (CT) excited state in **PBI-SST**.^{S7-S9} Furthermore, it is well-established in literature that locally excited states of PBI derivatives typically exhibit high photoluminescence quantum yield (PLQY) values, attributed to their large transition dipole moment and nearly complete orbital overlap.^{S8,S9} The **PBI-SST** compound, specifically in chloroform, demonstrated an impressive PLQY of 88%, underscoring the highly emissive nature of the Hybridized Locally Excited and Charge Transfer (HLCT) state.

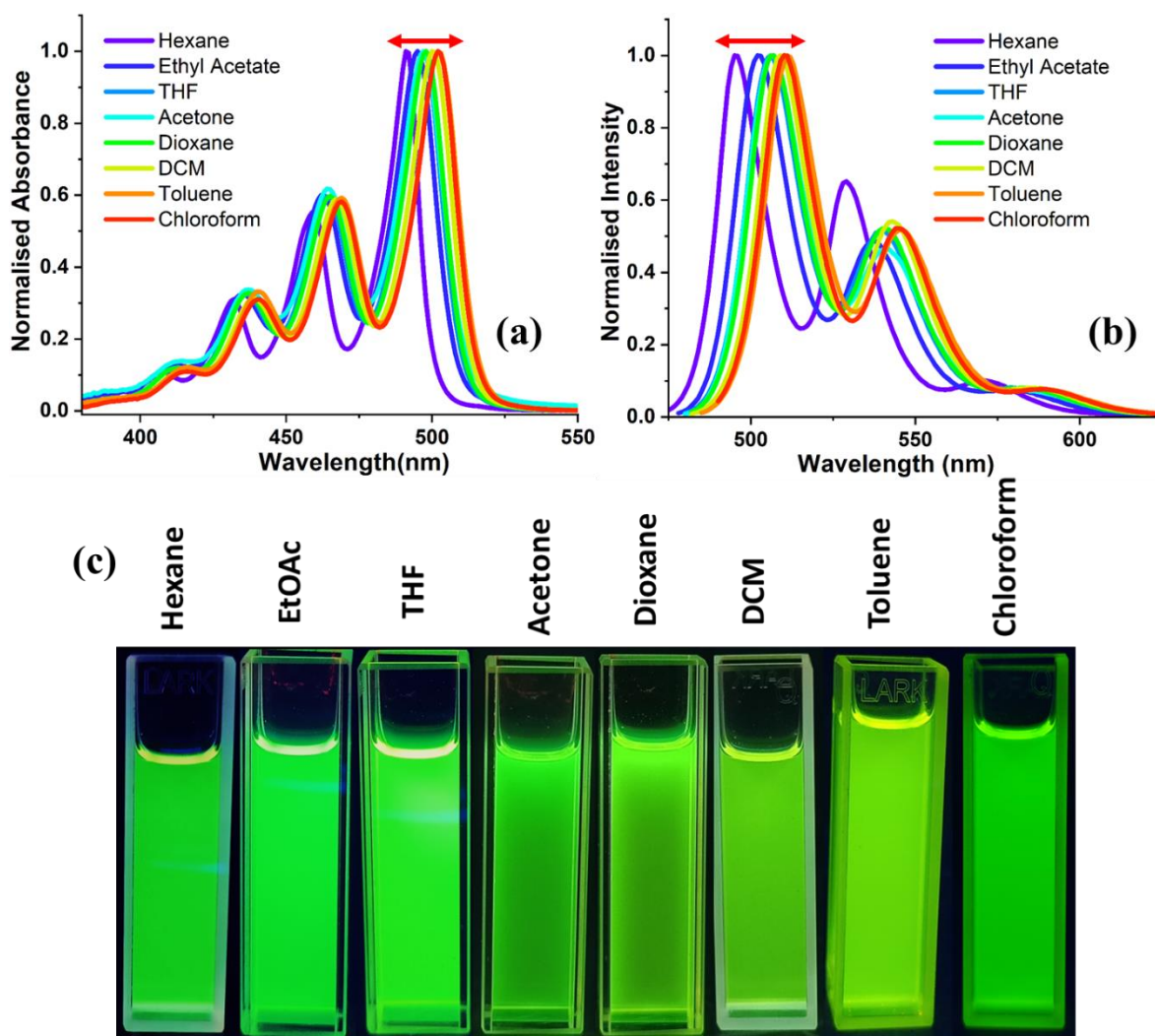


Figure S25. Absorption (a) and Fluorescence (b) spectra of compound **PBI-SST** obtained in a diverse range of solvents; (c) Solution state images of **PBI-SST** in a diverse range of solvents.

Table S7. Photophysical properties of **PBI-SST** in a diverse range of solvents varying with polarity.

Solvent	Absorption (nm)	Emission (nm)
Hexane	490	495
EtOAc	495	502
THF	497	506
Acetone	497	506
Dioxane	498	507
DCM	500	509
Toluene	502	511
Chloroform	502	510

18. Time resolved photoluminescence studies

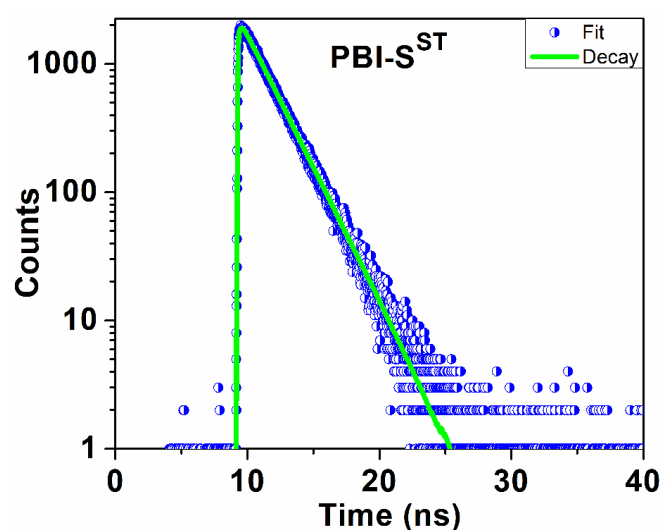


Figure S26. Fluorescence lifetime decay spectra of emitter **PBI-SST** in chloroform; Experimental decay in red-coloured circles; Mono-exponential fit in blue coloured line.

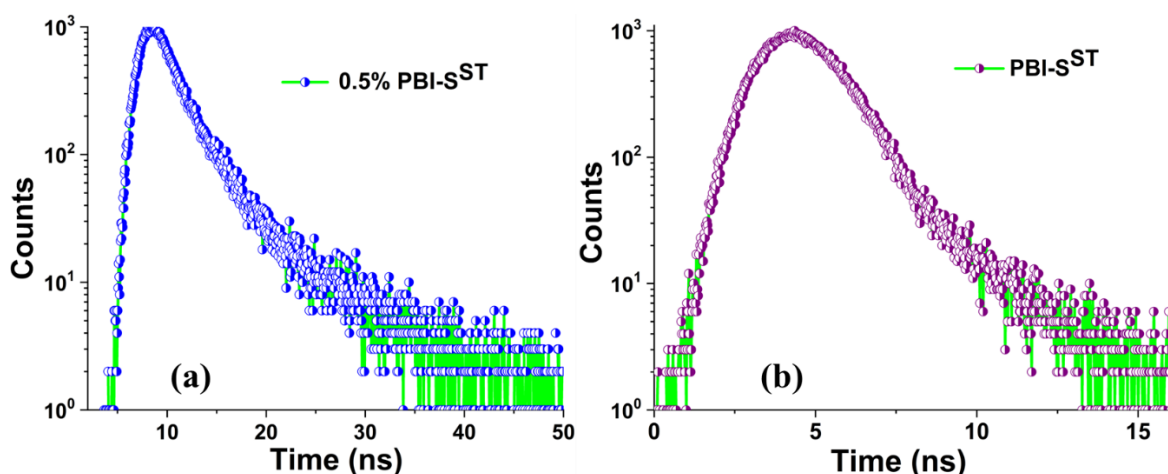


Figure S27. Fluorescence lifetime decay spectra of emitter **PBI-SST** in undoped state (a); and in doped state (5 wt% CBP) (b).

The detailed quantum chemical calculations including natural transition orbitals, singlet-triplet energy levels and transition density matrix calculations for the perylene based emitter **PBI-SST** supports the locally excited dominant HLCT character as also reported earlier for the perylene based emitters.^{S10} In addition, mono-exponential fluorescence decay lifetime (Fig. S26) further reinforced our findings. In case of planar molecular structures, triplet-triplet annihilation (TTA) can also be responsible for the high exciton utilization efficiency. In the present case the overall structure of the **PBI-SST** molecule is not exactly planar as can be seen from the optimized structure as provided in the Figure S19a, b.

19. References

- S1. Siddiqui, A., Thawarkar, S. and Singh, S.P., A novel perylene diimide molecule: Synthesis, structural property relationship and nanoarchitectonics, *J. Solid State Chem.* **2022**, 306, 122687.
- S2. Rocard, L., Hatych, D., Chartier, T., Cauchy, T. and Hudhomme, P., Original Suzuki–Miyaura Coupling Using Nitro Derivatives for the Synthesis of Perylene diimide-Based Multimers, *Eur. J. Org. Chem.* **2019**(47), 7635–7643.
- S3. N. Godbert, A. Crispini, M. Ghedini, M. Carini, F. Chiaravallotti, and A. Ferrised, *J. Appl. Cryst.*, 2014, 47, 668–679.
- S4. a) Gaussian 09, Revision B.01, M. J. Frisch, G. W. Trucks, H. B. Schlegel, G. E. Scuseria, M. A. Robb, J. R. Cheeseman, G. Scalmani, V. Barone, B. Mennucci, G. A. Petersson, H. Nakatsuji, M. Caricato, X. Li, H. P. Hratchian, A. F. Izmaylov, J. Bloino, G. Zheng, J. L. Sonnenberg, M. Hada, M. Ehara, K. Toyota, R. Fukuda, J. Hasegawa, M. Ishida, T. Nakajima, Y. Honda, O. Kitao, H. Nakai, T. Vreven, J. J. A. Montgomery, J. E. Peralta, F. Ogliaro, M. Bearpark, J. J. Heyd, E. Brothers, K. N. Kudin, V. N. Staroverov, R. Kobayashi, J. Normand, K. Raghavachari, A. Rendell, J. C. Burant, S. S. Iyengar, J. Tomasi, M. Cossi, N. Rega, J. M. Millam, M. Klene, J. E. Knox, J. B. Cross, V. Bakken, C. Adamo, J. Jaramillo, R. Gomperts, R. E. Stratmann, O. Yazyev, A. J. Austin, R. Cammi, C. Pomelli, J. W. Ochterski, R. L. Martin, K. Morokuma, V. G. Zakrzewski, G. A. Voth, P. Salvador, J. J. Dannenberg, S. Dapprich, A. D. Daniels, O. Farkas, J. B. Foresman, J. V. Ortiz and J. Cioslowski Fox, *D. J. Gaussian Inc., Wallingford, CT*, **2009**; b) C. Lee, W. Yang and R. G. Parr, *Phys. Rev. B*, **1988**, 37, 785–789; c) A. D. Becke, *J. Chem. Phys.*, **1993**, 98, 1372–1377.
- S5. Liu, T., Zhu, L., Gong, S., Zhong, C., Xie, G., Mao, E., Fang, J., Ma, D. and Yang, C., A red fluorescent emitter with a simultaneous hybrid local and charge transfer excited state and aggregation-induced emission for high-efficiency, low efficiency roll-off OLEDs. *Adv. Opt. Mater.*, **2017**, 5(13), 1700145.
- S6. C. A. Fuller, and C. E. Finlayson, Solvatochromism in perylene diimides; experiment and theory, *Phys. Chem. Chem. Phys.*, 2017, 19, 31781.
- S7. R. K. Konidena, K. J. Thomas, D. K. Dubey, S. Sahoo and J. H. Jou, A new molecular design based on hybridized local and charge transfer fluorescence for highly efficient (> 6%) deep-blue organic light emitting diodes, *Chem. Commun.*, 2017, 53, 11802–11805.
- S8. I. Bala, N. Singh, R. A. K. Yadav, J. De, S. P. Gupta, D. P. Singh, D. K. Dubey, J. H. Jou, R. Doualid, and S. K. Pal, Room temperature perylene based columnar liquid crystals as solid-state fluorescent emitters in solution-processable organic light-emitting diodes, *J. Mater. Chem. C*, 2020, 8, 12485–12494.
- S9. X. Tang, Q. Bai, Q. Peng, Y. Gao, J. Li, Y. Liu, L. Yao, P. Lu, B. Yang and Y. Ma, Efficient Deep Blue Electroluminescence with an External Quantum Efficiency of 6.8% and CIE_y < 0.08 Based on a Phenanthroimidazole–Sulfone Hybrid Donor–Acceptor Molecule, *Chem. Mater.*, 2015, 27, 7050–7057.

S10. Shen, Y., Zhang, Z., Liu, H., Yan, Y., Zhang, S., Yang, B. and Ma, Y., Highly efficient orange-red/red excimer fluorescence from dimeric π - π stacking of perylene and its nanoparticle applications, *J. Phys. Chem. C*, **2019**, *123*(20), 13047-13056.